Science Immunology
AAAS

Supplementary Materials for

Single-cell deletion analyses show control of pro–T cell developmental speed and pathways by Tcf7, Spi1, Gata3, Bcl11a, Erg, and Bcl11b

Wen Zhou *et al.*

Corresponding author: Ellen V. Rothenberg, evroth@its.caltech.edu

Sci. Immunol. **7**, eabm1920 (2022)
DOI: 10.1126/sciimmunol.abm1920

The PDF file includes:

Other Supplementary Material for this manuscript includes the following:

SUPPLEMENTARY MATERIALS AND METHODS

Mouse models

C57BL/6J (B6), B6.Cg-Tg(BCL2)25Wehi/J (Bcl2-tg), B6N.Cg-*Commd10*$^{Tg(Vav1–icre)A2Kio}$/J) (*Vav1*-iCre) and B6.Gt(ROSA)26Sor$^{tm1.1(CAG-cas9*,-EGFP)}$Fezh/J (Cas9) mice were bred in-house from stock purchased from the Jackson Laboratory (catalog numbers #000664, #002320, #018968, and #026179, respectively). For the Cas9 mice, animals from Jackson Laboratories stock #026179 were repeatedly backcrossed to B6 before use. B6.*Bcl11b*$^{yfp/yfp}$ reporter mice(*32*) were used for bulk RNA-seq analysis, and B6.*Bcl11b*$^{fl/fl}$ mice(*34*, *37*) were both reported previously. All mice were maintained on the B6 background and regularly genetically monitored. For CRISPR/Cas9 experiments, homozygous Bcl2-tg mice and homozygous Cas9 mice were crossed to generate B6-Cas9/+; +/Bcl2-tg heterozygotes for each experiment. For Bcl11b experiments, B6.Bcl11b$^{fl/+}$ *Vav1*-iCre heterozygous mice were bred to obtain *Bcl11b*$^{+/+}$ and *Bcl11b*$^{fl/fl}$ *ROSA26R-YFP* mice with *Vav1*-iCre, as previously described(*37*), which are denoted here as WT and Bcl11b KO. Bone marrow was taken from mice at 9.5-11.5 weeks of age. Thymus samples were taken from mice at 4-5.5 weeks of age. Animals used for these experiments were bred and maintained at the Animal Facilities at the California Institute of Technology under conventional Specific Pathogen-Free conditions, and animal protocols were reviewed and approved by the Institute Animal Care and Use Committee of California Institute of Technology (Protocol #1445-18G).

Cell lines

To provide a microenvironment that supports T-lineage differentiation *in vitro*, we co-cultivated purified BM cells with the OP9-DLL1 or OP9-DLL4 stromal cell lines(*6*), which were originally obtained from J. C. Zúñiga-Pflücker (Sunnybrook Research Institute, University of Toronto), or with MS5-mDLL1 or MS5-mDLL4 stromal cells(*14*), which were obtained from Dr. Gay Crooks (UCLA) and maintained in our laboratory as described in the

original reference(*14*). Details of the differentiation cultures are given below under BM Cell Differentiation.

CELL PURIFICATION AND CULTURE

Primary Cell Purification

For *in vitro (ex-vivo)* differentiation of pro-T cells, bone marrow hematopoietic progenitors were used for input. Bone marrow (BM) was removed from the femurs and tibiae of 10-12 week-old mice. To generate precursor-enriched populations as input for T-cell differentiation culture, suspensions of BM cells were prepared and stained for lineage markers using biotin-conjugated lineage antibodies: CD3ε (eBioscience, clone 145-2C11), CD19 (eBioscience, clone 1D3), B220 (eBioscience, clone RA3-6B2), NK1.1 (eBioscience, clone PK136), CD11b (eBioscience, clone M1/70). CD11c (eBioscience, clone N418), Gr1 (eBioscience, clone RB6-8C5), and Ter119 (eBioscience, clone TER-119). They were then incubated with streptavidin-coated magnetic beads (Miltenyi Biotec), and passed through a magnetic column (Miltenyi Biotec), with the flow-through cells denoted as 'Lin$^-$ BM'.

For all scRNA-seq experiments in this study, the freshly isolated Lin$^-$ BM cells were immediately further FACS sorted to purify live (7AAD^{negative}), CD45$^+$ "LSK" cells (Lin^{negative} Scal^{high} c-Kit^{high}), as described in the section "Flow Cytometry and Cell Sorting", as a more stringently purified source of multipotent hematopoietic stem and progenitor cells. All the BM precursors used (Lin$^-$ or LSK) were frozen in liquid nitrogen for storage in freeze-down medium containing 10% DMSO, 40% FCS and 50% OP9 medium (defined below under "BM cell differentiation") before initiating any differentiation assays.

Flow Cytometry and Cell Sorting

Unless otherwise noted, flow cytometry analysis and FACS of all samples were carried out using the procedures outlined. Briefly, cultured cells on tissue culture plates and primary cells from thymus were prepared as single cell suspensions, incubated in 2.4G2 Fc blocking

solution, stained with respective surface cell markers as indicated, resuspended in Hanks Buffered Saline Solution (HBSS) supplemented with 10% FBS and 10 mM HEPES, and filtered through a 40 μm nylon mesh. They were then analyzed using a benchtop MacsQuant flow cytometer (Miltenyi Biotec, Auburn, CA) or sorted with a Sony Synergy 3200 cell sorter (Sony Biotechnology, Inc, San Jose, CA) or with a FACSAria Fusion cell sorter (BD Biosciences). All antibodies used in these experiments are standard, commercially available monoclonal reagents widely established to characterize immune cell populations in the mouse. Acquired flow cytometry data were all analyzed with FlowJo software (Tree Star). For FACS purification of the Lin^- $Sca\text{-}1^+$ $c\text{-}Kit^+$ subset of bone marrow cells as input, Lin-depleted BM cells derived from each animal and each time point were stained with fluorescently conjugated streptavidin to gate out residual Lin^+ cells, and with fluorescent conjugated antibodies against Sca-1 (eBioscience, clone D7) and c-Kit (eBioscience, clone 2B8). To purify DN cells, differentiating T lineage cells derived from each animal and each time point were first stained with a biotin-conjugated lineage cocktail (TCRβ (eBioscience, clone H57-597), TCRγδ (eBioscience, clone GL-3), and CD19, NK1.1, CD11b, CD11c, and Gr1 as above). Secondary surface staining was performed with fluorescently conjugated streptavidin to gate out Lin^+ cells, and fluorescent conjugated antibodies against CD45, c-Kit (eBioscience, clone 2B8), CD44 (eBioscience, clone IM7), CD25 (eBioscience or Biolegend, clone PC61.5), and in some experiments Thy1.2 (Biolegend, clone 53-2.1). Viability dye 7AAD (eBioscience) was applied to exclude dead cells. Usually streptavidin-PerCP, Kit-APC, Sca-1-PE, CD45-e450 or CD45-PECy7, CD44-E450, and CD25-APC-e780 conjugates were used, to avoid interference with the CFP (mTurquoise) fluorescence of the gRNA vector or the YFP (mCitrine) fluorescence of the *Bcl11b*$^{yfp/yfp}$ reporter, as appropriate. Details are repeated below in descriptions of individual experiments.

BM Cell Differentiation

For standard differentiation of pro-T cells, the hematopoietic progenitors were thawed and either cultured on OP9-DLL1 or OP9-DLL4 monolayers using OP9 medium (α-MEM, 20%

FBS, 50 μM β-mercaptoethanol, Pen-Step-Glutamine) supplemented with 10 ng/ml of IL-7 (Pepro Tech Inc) and 10 ng/ml of Flt3L (Pepro Tech Inc); or aggregated to artificial thymic organoids with ATO-mDLL1 or ATO-mDLL4, seated at the air-medium interface on a culture insert (Millipore Sigma) in serum-free ATO medium (DMEM-F12, 2X B27, 30 μM Ascorbic acid, Pen-Step-Glutamine) supplemented with 5 ng/ml of IL-7 (Pepro Tech Inc) and 5 ng/ml of Flt3L (Pepro Tech Inc). If viral delivery of gRNA was required at the start of the culture, thawed BM precursors were initially incubated for 20-24 hours in OP9 medium supplemented with 10 ng/ml of SCF (Pepro Tech Inc), 10 ng/ml of IL-7 (Pepro Tech Inc) and 10 ng/ml of Flt3L (Pepro Tech Inc), without stromal cells, to launch the cells into cycle. This primed them for retroviral transduction before initiating co-culture with the stromal cells, as detailed below in the following section.

CRISPR/Cas9-mediated Acute Deletion in Precursor Cell Cultures

To generate input cells, Cas9 mice were first bred to Bcl2-tg mice to generate heterozygotes for both transgenes. Bcl2-transgenic mice were used to preserve the viability of cells undergoing alterations of development under regulatory perturbation(*65*, *66*), which is essential in order to measure the gene expression changes that are responsible for the change. We have previously shown that the Bcl2 transgene does not affect normal T cell development in vivo(*4*), and Fig. S3 shows further evidence via single-cell transcriptomes that the Cas9;Bcl2-tg control cells develop in culture very similarly to wildtype, nontransgenic B6 pro-T cells developing in vivo.

LSK or Lin^-BM cells from these Cas9;Bcl2-tg animals were purified and stored as described above. 20-24 hours after thawing and recovery in cytokines, the cells were transduced with retroviral vectors encoding reporters (CFP) and the indicated guide RNAs (sgRNAs) as detailed below, and then seeded to OP9-DLL1 culture. The methods used to generate the virus supernatant and infecting BM cells were described previously(*39*). For infecting LSK precursors for scRNA-seq (CRISPR), different batches of virus were first tested on primary BM precursors to determine the accurate titers (Fig. S12B), and then delivered to target cells in the actual CRISPR pool perturbation experiments at a precise multiplicity of

infection (MOI) of 0.5 or 1. For cell-surface phenotypic assays, cells were analyzed after 2-6 days after culture. For scRNA-seq, retrovirus infected $Lin^{-}CD45^{+}c\text{-}Kit^{hi}CFP^{+}$ cells were sorted preparatively on a FACSAria Fusion cell sorter (BD Biosciences).

CONSTRUCT DESIGN AND CLONING

Cloning

The retroviral vector backbone used for sgRNA expression cloning was based on previously published E42-dTet(*39*) with the following modifications: 1) Capture sequence 1 (Cap1) was added to the sgRNA scaffold before the termination signal. 2) One nucleotide 'G' was deleted before the sgRNA protospacer insertion site (two *AarI* restriction enzyme cutting sites) to allow compatibility with dual sgRNA vector cloning. The cloning was achieved through high-fidelity PCR (primers as shown below) and Gibson assembly, final cloned product containing the human U6 (hU6) promoter, two *AarI* cutting sites, gRNA backbone with Cap1 sequence and mTurquoise2 fluorescent marker, was as shown in bottom middle in Fig.1D.

For dual sgRNA cloning, a 'donor' sequence containing gRNA backbone and mouse U6 (mU6) promoter were obtained from a plasmid modified from Vidigal et al. (*63*). Specifically, the capture sequence 2 (Cap2) were added prior to the termination signal of the sgRNA scaffold backbone; we also found the linker sequence between gRNA backbone and mU6 promoter contained a partial sgRNA backbone sequence that hinders the PCR capability and Gibson assembly accuracy, therefore we cloned to remove the partial repeat sequence in the linker region. The cloning was performed through sequential high-fidelity PCR (primers as listed below) and blunt end ligation.

The pool-based dual gRNA cloning was performed similarly to the protocol described in ref. (*63*) with the modified vector and plasmids above (workflow shown in Fig. 1D), and with minor protocol modifications as follow. 1) the 'Donor sequence' containing gRNA scaffold - Cap2 - modified linker – mU6 were obtained through PCR with the modified plasmid, rather than enzymatic digestion. 2) All gel purification steps were avoided, and purifications were

achieved with Ampure XP or SPRIselect beads (Beckman Coulter) instead. 3) Selected gRNAs from the oligopool were qPCR quantified before and after the pool-based vector cloning process (Fig. S12A) for quality control, ensuring the amplification evenness of the final plasmid pool. 4) A retroviral vector was used instead of lentiviral vectors.

Primers used in cloning

Primers for E42 modification and addition of Cap1	
backbone_fwd	GCTTTAAGGCCGGTCCTAGCAATTTTTTTCTCGAGTGGCTC
backbone_rev	TGTGTTCACCTGCGAGCGGTGTTTCGTCCTTTCCACAAG
insert and loop_fwd	ACCGCTCGCAGGTGAACACAACA
insert and loop_rev	TTGCTAGGACCGGCCTTAAAGCGCACCGACTCGGTGCCAC
Primers for donor mU6 modifications and addition of Cap2	
pD_mU6_rev_cap2_blunt	GCTAATAGGTGAGCGCACCGACTCGGTGCCAC
pD_mU6_fwd_cap2_blunt	GGCTAAGGTTTTTTGTTTTAGAGCTAGAAATAGCAAGTTAAA ATAAGGCTAGTC
rev_del_partial_primer	AAAAAACCTTAGCCGCTAATAGGTGAG
fwd_del_partial_primer	TTTAGCGCGTGCGCCAATTC
Primers for pool-based dual gRNA vector assembly	
Fwd lib amp primer	GTTTTGAGACTATAAATATGCATGCGAGAAAAGCCTTGTT
Rev lib amp primer	GACTAGCCTTATTTTAACTTGCTATTTCTAGCTCTAAAAC
Fwd pDonor opening	GTTTTAGAGCTAGAAATAGCAAGTT
Rev pDonor opening	CAAACAAGGCTTTTCTCGCA

sgRNA sequence design and oligo pool design

sgRNAs were designed using GPP sgRNA Designer for CRISPRko (by Broad Institute(*67*, *68*)) and GUIDES(*69*) (Sanjana lab) in combination. Specifically, the 3 pairs of sgRNAs of each gene were picked from the top ranked, non-overlapping gRNAs from list generated from GPP designer (https://portals.broadinstitute.org/gpp/public/analysis-tools/sgrna-design). Each pair are designed to target the same exon of the same gene, preferably at or upstream of exons with functional annotation. If GPP designer did not generate all pairs of gRNA sequences desired, GUIDES tool (http://guides.sanjanalab.org/) was used following the instruction. Both designer tools were based on target genome of Mouse GRCm38 and SpyoCas9 (NGG). For oligo pool synthesis, the 110nt oligos were designed and synthesized as follows:

5'—[CATGCGAGAAAAGCCTTGTTTGG]—[gRNA1]—
[GTTTGGGTCTTCGAGAAGACCTCACCG]—[gRNA2]—
[GTTTTAGAGCTAGAAATAGC]—3'

Because the circular DNA will be digested with restriction enzyme *BbsI*, 2 cutting sites of *BbsI* are incorporated in the middle sequence between gRNA1 and gRNA2. Before assembling the sequence of the designed oligo pool, we made sure that the gRNA1, gRNA2 and junction sequences with the left and right primer handles didn't introduce additional *BbsI* binding sites ('GAAGAC', 'GTCTTC'). For control sequences, we included a pair of non-targeting control sequences from mouse GeCKO library A(*70*), one pair of sgRNA sequences designed against a non-expressing gene Hes3. Note that the final cloning product of the vector library also included a third detectable nontargeting vector that was actually from residual un-cut vector backbone. Cells found to be infected with this construct were included among the 'controls' in the differential gene expression analysis but not included in the comparison of differential cell recovery, because their level of representation in the initial pool was unknown. Details of the 110nt designed oligo pool sequences and gRNA sequences are included in Table S10.

RNA-SEQ AND SINGLE-CELL RNA-SEQ METHODS

Bulk RNAseq Analysis for in vivo vs. in vitro reference analysis

For the test of *in vitro* vs. *in vivo* comparability (Fig. S1), Lin^- BM cells were harvested from B6.*Bcl11b*$^{yfp/yfp}$ animals, and cultured in differentiation conditions for five or six days as described above (BM Cell Differentiation). Upon harvesting, cells were subdivided into $CD44^{hi}$ $CD25^{low}$ for DN1, $CD44^{hi}$ Bcl11b-YFP^{neg} $CD25^{hi}$ for DN2a, and $CD44^{hi}$ Bcl11b-$YFP^{pos}CD25^{hi}$ DN2a (newly committed DN2a/2b transitional cell) fractions by sorting as described(*32*). The "DN1" populations were highly enriched for ETP cells. As c-Kit staining can show reduced dynamic range on cells differentiating *in vitro*, *Bcl11b* expression provides a superior marker for the timing of commitment(*32*). This separation was followed by RNA purification following the instructions of the RNeasy Micro Kit (Qiagen 74004). cDNA from each sample was prepared using NEBNext Ultra RNA Library Prep Kit for Illumina (E7530, NEB). All bulk libraries were sequenced on Illumina HiSeq2500 in single read mode with the read length of 50 nt. Base calls were performed with RTA 1.13.48.0 followed by conversion to FASTQ with bcl2fastq 1.8.4 and produced approximately 30 million reads per sample.

RNA-seq reads were mapped onto the mouse genome build GRCm38/mm10 using STAR (v2.4.0) and were post-processed with RSEM (v1.2.25; http://deweylab.github.io/RSEM/) according to the settings in the ENCODE long-rna-seq-pipeline (https://github.com/ENCODE-DCC/long-rna-seq-pipeline/blob/master/DAC/STAR_RSEM.sh), with the minor modifications that the setting '–output-genome-bam–sampling-for-bam' was added to rsem-calculate-expression. STAR and RSEM reference libraries were created from genome build GRCm38/mm10 together with the Ensembl gene model file Mus_musculus.GRCm38.gtf. The resulting bam files were used to create HOMER tag directories (makeTagDirectory with –keepAll setting). For analysis of statistical significance among DEGs, the raw gene counts were derived from each tag directory with 'analyzeRepeats.pl' with the '–noadj -condenseGenes' options, followed by the 'getDiffExpression.pl' command using EdgeR (v3.6.8; http://bioconductor.org/packages/release/bioc/html/edgeR.html). For data visualization, RPKM normalized reads were derived using the 'analyzeRepeats.pl'

command with the options '–count exons –condenseGenes –rpkm'; genes with an average of RPKM ≥1 across samples were kept, and their RPKM values were processed by log transformation. The normalized datasets were then hierarchically clustered with R hclust function based on Euclidean distance and 'complete' linkage. The heatmap is visualized with R pheatmap with $\log_2$ transformed RPKM data (after adding 0.1 to all values).

Single Cell RNA-seq comparing *in vitro* with *in vivo* pro-T cells (10X Chromium V2)

Note that only the scRNA-seq data from Fig. S2 was obtained through 10X Chromium 3' capture V2, the rest of the scRNA-seq data were obtained through the 3' capture V3 chemistry.

The early T cells derived in ATO-DLL4 from LSK were sorted as shown in Fig. S2A (bottom). The sample was then washed and resuspended to 1 million cells/mL concentration in HBSS supplemented with 10% FBS and 10 mM HEPES, 17,400 cells were loaded into a 10X Chromium v2 lane, and the subsequent preparation was conducted following the instruction manual of 10X Chromium v2. The cDNA library and final library after index preparation were checked with bioanalyzer (High Sensitivity DNA reagents, Agilent Technology #5067-4626; Agilent 2100 Bioanalyzer) for quality control. Following the library preparation, the sequencing was performed with paired-end sequencing of 150nt each end on one lane of HiSeq4000 per sample, by Fulgent Genetics, Inc. (Temple City, CA). The reads were mapped onto the mouse genome Ensembl gene model file Mus_musculus.GRCm38.gtf using a standard CellRanger pipeline. Cells were sequenced to a targeted depth of 50,000 reads per cell.

Direct-capture Pool-perturbation scRNA-seq (with 10X Chromium V3)

LSK were purified, recovered in cytokines and infected with MOI 0.5-1, and cultured with OP9-DL1 as described above. Note that two separate packagings of the viral pools were infected into cells at MOI=1.0 or MOI=0.5, in parallel, in separate wells, to serve as biological replicates. The cells infected with independently packaged viruses were cultured

separately, in parallel, until harvest, when they could be hashtagged and then finally combined for a pooled scRNA-seq analysis. This strategy was designed to allow capture of a full range of genuine biological response variation among the separate replicates while precluding technical batch effects at the analytical stage.

The medium was changed on day 3. On day 5, the cells were harvested through scraping, filtered and prepared for FACS sorting as described above. Specifically, cells derived from each animal and each time point were stained with a biotin-conjugated lineage cocktail (TCRβ (ebioscience, clone H57-597), TCRγδ (eBioscience, clone GL-3), CD19, NK1.1, CD11b, CD11c, and Gr1). Secondary surface staining was performed with fluorescently conjugated streptavidin, CD45, c-Kit (eBioscience, clone 2B8), CD44 (eBioscience, clone IM7), CD25 (eBioscience or Biolegend, clone PC61.5), and TotalSeq A (Biolegend) anti-Mouse Hashtag 1-6 (1:50, in separate infected samples). A viability dye 7AAD (eBioscience) was again applied to exclude dead cells. The sorted cells ($CD45^{positive}Lin^{low}7AAD^{negative}CFP^{high}c\text{-}Kit^{positive}$) washed 2 times with HBSS supplemented with 10% FBS and 10 mM HEPES, pooled to target equal cell number from each Hash-tagged sample, and loaded onto one lane of a 10X Chromium V3 chip. The cDNA preparation was performed following the instruction manual of 10X Chromium v3 for perturbation with minor modifications, and the hashtag library was prepared following the Biolegend TotalseqA guide. The cDNA, gRNA library, Hashtag library, and final libraries after index preparation were checked with bioanalyzer (High Sensitivity DNA reagents, Agilent Technology #5067-4626; Agilent 2100 Bioanalyzer) for quality control. All libraries were sequenced on HiSeq4000, by Fulgent Genetics, Inc. Cells were sequenced to at least medium depth of 50,000 reads per cell for cDNA, 20M reads/sample for hashtags and 20M reads/sample for gRNAs.

Dual gRNA validation

gRNA2 with cap2 sequence were poorly detected in the pool based perturb-seq setup. We validated the efficiency of gRNA perturbation at position 2 and the dual gRNA perturbation efficacy compared to single gRNA. Specifically, 2 different sgRNA sequences against Il2ra

(encoding CD25) were designed, sequences as shown below. Dual gRNA vectors were constructed with combinations of the two gRNAs against CD25 as well as two non-targeting control sequences, as shown in Fig. S12C.

CD25 gRNA1: AGATGAAGTGTGGGAAAACG

CD25 gRNA2: CAAGAGAATCTATCATTTCG

Cont 1: GCGAGGTATTCGGCTCCGCG

Cont 2: GCTTTCACGGAGGTTCGACG

The dual vectors on the same retroviral backbone were packaged individually and delivered to Cas9 expressing Lin^- BM precursors for acute knockout, as described above. The cells were cultured for 6 days on OP9-DL1, and analyzed with flow cytometry. Specifically, cells were first stained with a biotin-conjugated lineage cocktail (TCRβ, TCRγδ, CD19, NK1.1, CD11b, CD11c, and Gr1). Secondary surface staining was performed with fluorescently conjugated streptavidin, CD45, c-Kit (eBioscience, clone 2B8), CD44 (eBioscience, clone IM7), CD25 (eBioscience or Biolegend, clone PC61.5), Thy1.2 (Biolegend, clone 53-2.1), and viability dye 7AAD (eBioscience) was again applied to exclude dead cells. The CD25 surface expression were quantified within the $7AAD^-Lin^-CD45^+CFP^+Thy1.2^+$ population, from each vector, as shown in Fig. S12D. The result confirmed that normally 99% of this population express CD25, and a single gRNA can lead to 70-90% perturbation outcomes. The position 2 on the vector, despite being poorly detected, was surprisingly more effective than position 1 in terms of perturbation efficacy. Importantly, dual gRNAs were consistently more effective in perturbation than the single gRNA vectors. Interestingly, a recent study by Replogle et. al.(*18*) has mentioned the preference of incorporating capture sequence 1 into the gRNA backbone stem loop instead of before the termination sequence to improve the efficiency of perturbation for pool-based CRISPRi scRNA-seq analysis. We have therefore also made the retroviral vector backbone with cap1 moved to the stem loop region, and the perturbation efficiency is pending future validation.

Single Cell RNA-seq (10X Chromium V3) for comparison of Bcl11b KO and WT Samples with Cell Hashing

LSK from Bcl11b WT and KO animals were obtained, aliquoted into 6-7k cell/tube, and stored in liquid nitrogen as described above (individual animals were not pooled). To setup the culture, cells were thawed and aggregated with MS5-mDLL4 (800-1000 LSK and 150k MS5-DLL4 cells per ATO), and seeded on culture inserts as described above. The ATO medium was changed every 3-4 days. After culturing for 10-13 days (note experiment 1 had only D10, and experiment 2 had both D10 and D13), the ATO was mechanically disrupted and *ex-vivo* derived T cells were prepared for FACS sorting as described above. Specifically, cells derived from each animal and each time point were stained with a biotin-conjugated lineage cocktail (TCRγδ (eBioscience, clone GL-3), CD19, NK1.1, CD11b, CD11c, and Gr1). Secondary surface staining was performed with fluorescently conjugated streptavidin, CD45, c-Kit (eBioscience, clone 2B8), CD44 (eBioscience, clone IM7), CD25 (eBioscience or Biolegend, clone PC61.5), and TotalSeq A (Biolegend) anti-Mouse Hashtag 1-8 (1:50, in separate samples). A viability dye 7AAD (eBioscience) was applied to exclude dead cells. The sorted cells ($CD45^{positive}Lin^{low}7AAD^{negative}CD25^{positive}$) washed 2 times with HBSS supplemented with 10% FBS and 10 mM HEPES, pooled to target equal cell number from each Hash-tagged sample, and loaded onto one lane of a 10X Chromium V3 chip. The cDNA preparation was performed following the instruction manual of 10X Chromium v3, and the hashtag library was prepared following the Biolegend TotalseqA guide. The cDNA, tag library, and final library after index preparation were checked with bioanalyzer (High Sensitivity DNA reagents, Agilent Technology #5067-4626; Agilent 2100 Bioanalyzer) for quality control. The cDNA final libraries was sequenced on HiSeq4000 or NovaSeq 6000, and the tag library was sequenced on HiSeq4000, by Fulgent Genetics, Inc. Cells were sequenced to an average depth of 50,000-70,000 reads per cell for cDNA and ~2,500 reads per cell for hashtags.

DATA ANALYSIS

Mapping of scRNA-seq Sequences, Hashtag and gRNA Identification

Single-cell RNA-seq data were processed using 10X Cellranger 3.0.0 software. Standard cellranger-mm10-3.0.0 reference annotations were loaded to the pipeline for read mapping and gene quantification.

To process single-cell hashtag and guide RNA sequencing data, two ultrafast in-house tools (**hashtag_tool** and **guiderna_tool**) (https://github.com/gaofan83/single_cell_perturb_seq/releases/tag/v.1.0.0) were developed to process raw fastq data and generate count tables (Fig.S12E). The results are typically delivered within one minute. Downstream R codes can be used to binarize the count tables for identity assignment using Gaussian Mixed Modeling.

As note, **guiderna_tool** was specifically developed for our dual-guide system with two guide-RNA sites (targeting different sites of the same gene) are engineered in the same vector backbone. Based on 10X bead chemistry, **Capture1** (5'-GCTTTAAGGCCGGTCCTAGCAA -3') and **Capture2** (5'-GCTCACCTATTAGCGGCTAAGG -3') sequences recognize expressed **Guide1** and **Guide2** RNA molecules that have reverse complement capture sequences inserted. Specifically, **Capture1** and **Capture2** sequences should pair with **Guide1** and **Guide2**, respectively. From in-house single-cell guideRNA data, UMI counts can be calculated for **Guide1** list of barcodes and **Guide2** list of barcodes. As note, **guiderna_tool** uses both capture sequences in R1 reads and template switching oligo sequence (TSO) in R2 read for read filtering and sorting; then potential **protospacer** sequences in R2 reads (after 5' TSO sequence) are mapped against the corresponding guide library (**Guide1** or **Guide2**) for quantification. In contrast, **Cellranger** finds a constant region after **protospacer** region in R2 first, then **protospacer** abundances in R2 are calculated. Since **guiderna_tool** utilizes both R1 and R2 read information for filtering, it is expected to be more accurate.

Gene and Cell Filtering, Data Alignment, and Clustering Analysis

The 10X Chromium V2 scRNA-seq analysis used to compare in vitro vs. in vivo-derived early pro-T cell samples (Fig. S2) was based on data filtered on cells with at least 1200 genes expressed (transcript count over 1); outliers with more than 4300 genes or 23k unique transcripts were removed (potential doublet) from the ATO scRNA-seq dataset, and outliers with more than 4400 genes or 27k unique transcripts were also removed from the thymocyte dataset (10X V2 run1 from ref.(*11*)), and only genes that were found expressed in at least 3 cells were kept in the analysis. The cells were further filtered to keep only cells with mitochondrial RNA content of less than 7.5-9%. These QC filters resulted in 6167 cells in the ATO scRNA-seq sample and 4783 cells in the thymocyte sample in Fig. S2. The top 3000 variable features were identified from each of the two datasets and integrated with CCA algorithm using the 3000 anchor features and 20 dimensions in Seurat v3(*71*). The principal component analysis was performed on the integrated dataset. In Fig.S2B, the UMAP1-2 display was analyzed based on PCs 1-20 of integrated data. In Fig.S2C-E, UMAP and clustering analyses were performed on integrated data after cell cycle regression according to Seurat 3 instruction. Louvain clustering was performed on the first 20 PCs with the resolution set to be 0.7.

For all the 10X Chromium V3 scRNA-seq datasets (all datasets in the study except in Fig.S2), analysis was based on data filtered on cells with at least 1300 genes expressed (transcript count > 1). The doublet elimination was guided through Cell Hashing. Specifically, the number of features vs. number of unique transcripts detected were plotted, and cells with more than 1 Cell Hashing tags were considered doublets and highlighted on the scatterplot. We dropped both the ‘cell hashing identified doublets’ and outliers with only one hashtag identified but which fell in the region of high numbers of gene detected and transcripts detected similarly to ‘cell hashing doublets’. The subsequent integration and clustering analysis were performed similarly described above, using Seurat 3. For the UMAP representation in Fig. 2, after UMI count matrices for all the samples were merged, scRNA-seq analysis was performed for cells with low mitochondrial content. Normalized UMI counts were further scaled with mitochondrial content and cell cycle stages regressed out using Seurat 3. (ref(*72*)). For the inter-dataset comparison of thymocytes (Accession number GSE137165) and control of perturbation subset in Fig. S3, similarly to Fig. S2, the

2000 integration features and 30 PCs were used for alignment of the two datasets through CCA using Seurat v3.

Unless specified, the trajectory and pseudo-time analysis with Monocle 3 were all performed on the cells that passed the filtering steps described above.

Kullback-Leibler (KL) Divergence Calculation

Kullback-Leibler (KL) divergence was used to compare two probability distributions. Here, we used it to calculate the pair-wise distance of samples based on cluster distributions of each sample. The number of cells in each cluster was counted in each sample, and the counts were aggregated and converted into a cluster distribution matrix. The pair-wise KL divergence matrix were computed with the KL function in philentropy (v 0.4.0) in R using the cluster distribution matrix, and the returned distance matrix is visualized in heatmap format with heatmap.2 using ggplots (v 3.1.0).

Pool-based CRISPR/Cas9 KO Assignment Strategy

The guide 1 and guide 2 identified using the in-house pipeline described above, were analyzed for agreement, as shown in Fig. S12F. The result shows general agreement between the paired guides designed, but guide2 UMI counts captured by capture 2 sequence were significantly lower than guide1-capture1, and were often undetected in individual cells. We validated that the guide2-capture2 were very efficient in generating KO phenotype (described above in Methods and in Fig. S12C-D), and Sanger sequencing of sampled plasmids confirmed good sequence quality of the guide1 and guide2 pairing (data not shown). Therefore, to maximize yield of cell numbers, in Fig. 1-4, we used guide1 assignment for gene perturbation identification. Specifically, the binarized gRNA assignment matrix was generated as described above, for guide1-capture1. The cells with 0 guide 1 assignment were represented as ‘unknown’, and 2 assignments or above were identified as ‘multi’ (for potential multiple vector infection). The 3 gRNA pairs (identified

through 3 singly infected guide RNA vectors) against the same genes were examined separately for analysis in Fig. 2F and S4C, and aggregated for gene specific KO effects in the rest of the analysis. The cells identified as ‘unknown’ or ‘multi’ (even with multiple infection against the same gene) were dropped from the analysis. Note that we noticed that Erg.3 vector produced slightly different perturbation outcome than the other 2 Erg vectors, therefore only cells with Erg.1 and Erg.2 gRNAs were selected and used to represent Erg KO in differential gene expression and SCENIC analysis.

Differential Gene Expression analyses

Genes differentially expressed between different sample classes within a population were defined (Table S3, Table S7) using Seurat 3 with standard criteria of qval < 1E-02, minimum fraction of cells expressing the gene ≥ 0.05, and natural log Fold-change (lnFC) between populations (using that pseudocount) ≥ 0.1. Note, in the analysis we used the default Seurat 3 pseudocount setting of 1, which reduces noise from low-level transcripts but compresses the dynamic range for comparisons between genes non-expressed and modestly expressed in two different populations. Given the robustness in identifying highly expressed genes’ differential expression pattern, the criteria described above were used for the DEG identification in the paper and for analyses derived from their relative expression levels (e.g. Fig. 3C,D, Fig. S5C-F, Fig. S9). Despite pseudocount of 1 being common practice, the choice of pseudocount is arbitrary and can introduce subtle bias in DEG analysis.

For some future analyses, however, greater sensitivity to differences in expression of lower-level transcripts could be desirable. Although setting pseudocounts close to zero arbitrarily increase the variance of genes with zero counts, we found that the fold change might better reflect lowly expressed transcription factors. Hence, we also provide a separate Table of differentially expressed genes calculated from the pool-perturbation CRISPR experiment using alternative criteria, with qval still <1E-02 and minimum fraction still ≥ 0.05, but with pseudocount set to 0.01 and minimum ln FC ≥ 0.2 (Table S11).

Single-cell RNA-seq DEG calling is nevertheless limited by the sparsity of the data due to inefficient transcript detection, with losses of statistical power for many genes, especially those lowly expressed. In cluster-to-cluster comparisons with limited cell numbers, this is even more problematic, making it difficult to use scRNA-seq DEG calls for any kind of causal network role inference for individual genes. The analyses in Fig. 8, Fig. S6G, H, Fig. S10F-H, Fig. S11, and Table S9 were made possible by intersecting our current results with previously-reported high sensitivity, robust DEG sets based on bulk population perturbation of Spi1 (PU.1) and Bcl11b (Table S9A,B). Individual Spi1 (PU.1)-affected DEGs were identified by their reciprocal responses to experimental gain of PU.1 at the DN2b/DN3 stage and to experimental disruption of Spi1 at the ETP-DN2a stage(*43*); only genes that met both criteria were included as PU.1-activated or PU.1-repressed DEGs for Fig. 8, Fig. S6G, H, Fig. S11, and Table S9D. Similarly, individual Bcl11b-affected DEGs in Fig. 8, Fig. S10F-H, Fig. S11, and Table S9B were identified by their overlapping responses to *Bcl11b* deletion under all three of the following conditions: Vav1-iCre induced deletion in vivo, Lck-Cre deletion in vivo, and Cas9-mediated deletion at the DN2b stage in vitro (*37*).

SCENIC Analysis and Visualization Graphics

We performed SCENIC(*38*) analysis on the scRNA-seq data without separating individual samples, following the workflow using the default parameters in SCENIC R setup. The co-expression network was generated using GENIE3(*73*), and potential direct-binding targets (regulons) were based on DNA-motif analysis. AUC, which identifies and scores gene regulatory networks or regulons in single cells, was calculated using AUCell as previously described(*38*). The motif bindings were inferred based on publicly available motif binding databases provided by the S. Aerts lab. Following the regulon calculation, the individual cells' regulon AUC values from 3.4_regulonAUC.Rds were extracted and separated by sample identity of perturbations based on gRNA assignment (CRISPR) or hashtags (Bcl11b). The AUC distributions of different genotypes were compared and analyzed for changes in regulon activity between different perturbations. Note that this SCENIC analysis

was completely independent of the definition of DEGs by Seurat 3, above. The full summary list of AUC values by samples for each KO are included in Tables S4 (CRISPR pool perturbation) and S8 (Bcl11b experiment 2).

Software Details

The bulk RNA-seq analysis were mapped with STAR (v2.4.0) and post-processed with RSEM (v1.2.25). The Fastq outputs for scRNA-seq data were aligned with Cellranger 3.0.0. The scRNA-seq downstream analysis were performed mainly in R (version 4.0.2) with the following packages: ggplot2(v3.3.2), dplyr(v1.0.2), cowplot(1.1.0), Seurat(v3.2.2), AUCell(v1.10.0), RcisTarget(v1.8.0), GENIE3(v1.10.0), SCENIC(v1.2.2), monocle3(v0.2.3.0), ggraph(v2.0.4), igraph(v1.2.6), philentropy (v 0.4.0), gplots (v 3.1.0). The statistical analyses were performed with methods as specified in the text using software mentioned above or with Graphpad Prism (v9.0.0).

Supplementary Figures and Legends

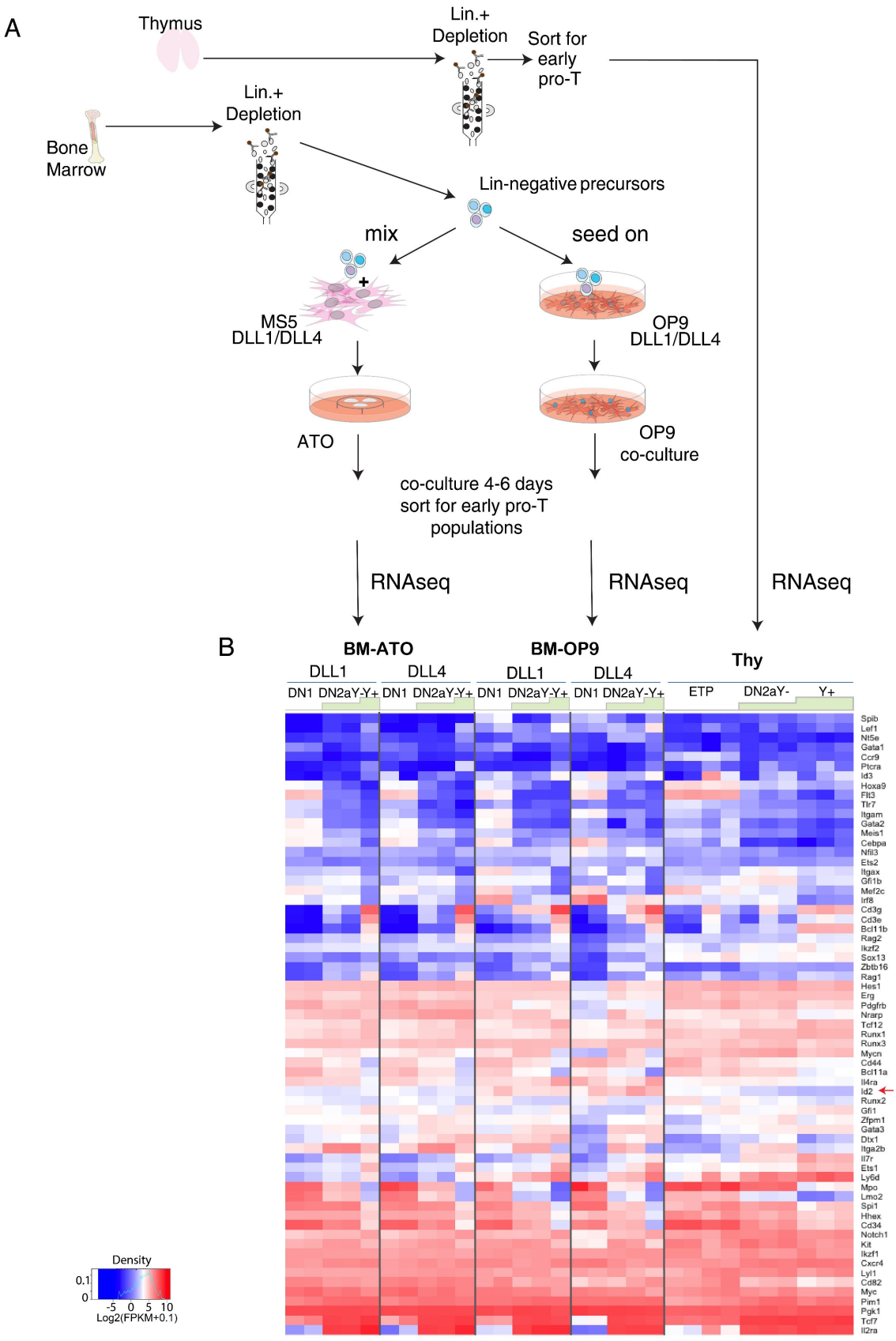
A
Thymus
Lin.+
Depletion
Sort for
early
pro-T
Bone
Marrow
Lin.+
Depletion
Lin-negative precursors
mix
seed on
MS5
DLL1/DLL4
OP9
DLL1/DLL4
ATO
OP9
co-culture
co-culture 4-6 days
sort for early pro-T
populations
RNAseq
RNAseq
RNAseq
B
BM-ATO
BM-OP9
Thy
DLL1
DLL4
DLL1
DLL4
DN1 DN2aY-Y+ DN1 DN2aY-Y+ DN1 DN2aY-Y+ DN1 DN2aY-Y+ ETP DN2aY- Y+
Spib
Lef1
Nt5e
Gata1
Ccr9
Ptcra
Id3
Hoxa9
Flt3
Tlr7
Itgam
Gata2
Meis1
Cebpa
Nfil3
Ets2
Itgax
Gfi1b
Mef2c
Irf8
Cd3g
Cd3e
Bcl11b
Rag2
Ikzf2
Sox13
Zbtb16
Rag1
Hes1
Erg
Pdgfrb
Nrarp
Tcf12
Runx1
Runx3
Mycn
Cd44
Bcl11a
Il4ra
Id2
Runx2
Gfi1
Zfpm1
Gata3
Dtx1
Itga2b
Il7r
Ets1
Ly6d
Mpo
Lmo2
Spi1
Hhex
Cd34
Notch1
Kit
Ikzf1
Cxcr4
Lyl1
Cd82
Myc
Pim1
Pgk1
Tcf7
Il2ra
Density
0.1
0
-5 0 5 10
Log2(FPKM+0.1)

Fig. S1. Bulk RNA-seq analysis of *in vivo* and *ex-vivo* derived early pro-T cells.

A) Illustration of early pro-T cells harvested from thymus or derived by *in vitro* differentiation from bone marrow (BM) precursors. The *in vitro* culture systems shown include both OP9-DL co-culture systems with OP9-DLL1 or OP9-DLL4 stromal cells, and 3D artificial thymic organoid (ATO) systems based on co-aggregation with MS5-mDLL1 or MS5-mDLL4 stromal cells, as detailed in Methods. *B)* Expression heatmap of bulk RNA-seq measurements, comparing corresponding subsets of early pro-T cells harvested *in vivo* with those sorted from *in vitro* differentiation of BM precursors in the culture systems as illustrated in A. DN1: $CD44^{+}$ $CD25^{-}$, representing highly ETP-enriched cells; $DN2aY^{-}$: Bcl11b-YFP-negative $CD44^{+}$ $CD25^{+}$, representing uncommitted DN2a cells. Y^{+}: Bcl11b-YFP^{+} $CD44^{+}$ $CD25^{+}$, representing newly committed DN2a and DN2b cells. Gating used Bcl11b rather than minor changes in Kit expression as a sharper criterion of commitment in these newly differentiating cells(*32*). All genes plotted are from a curated list of developmentally important regulatory genes described in a previous study(*11*). Color scales indicate raw expression levels as $\log_2$(RPKM+0.1), without row normalization. This provides a direct visualization of the full dynamic range of gene expression levels.

Figure S2

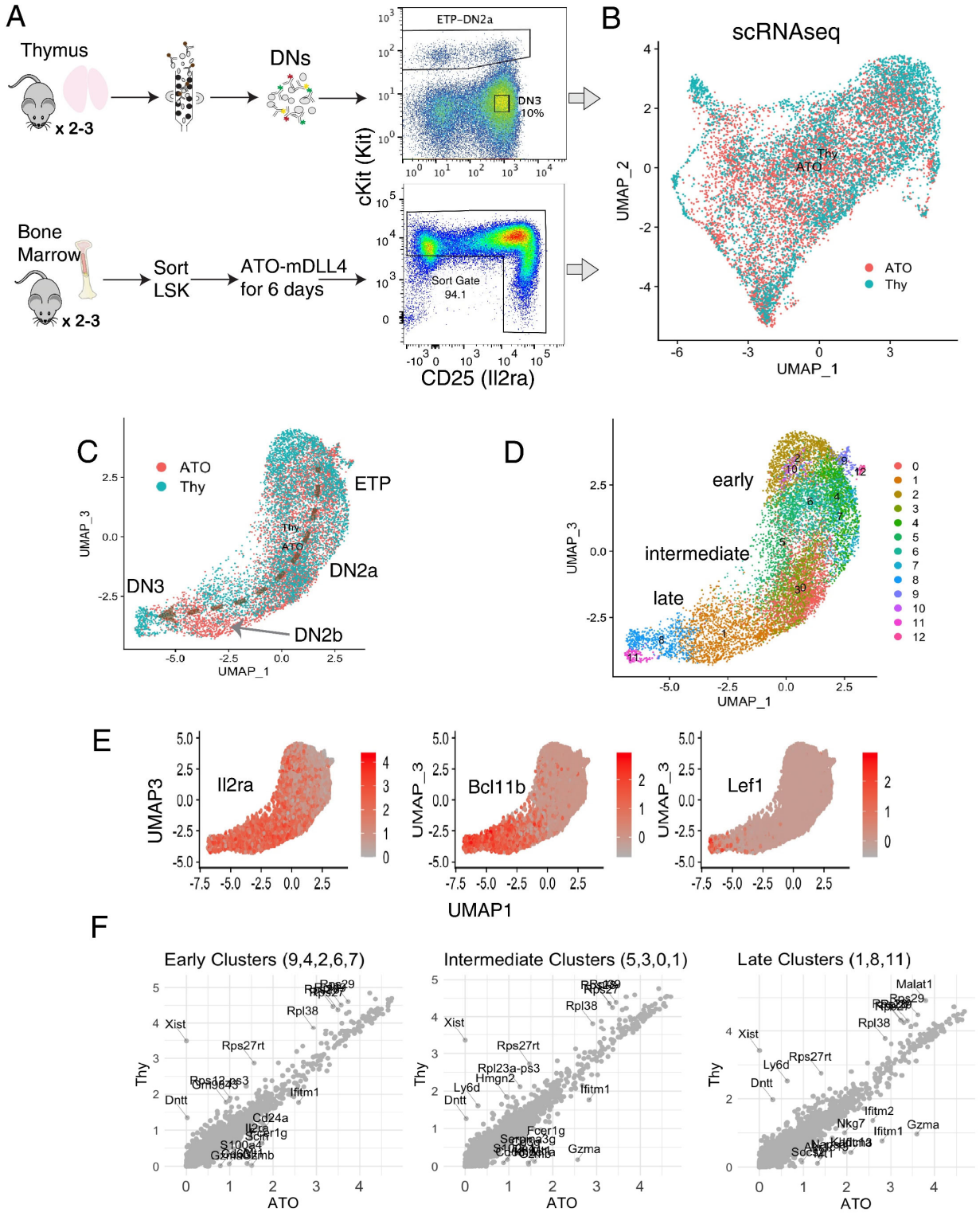
A
Thymus
x 2-3
DNs
Bone Marrow
x 2-3
Sort LSK
ATO-mDLL4 for 6 days
ETP-DN2a
DN3 10%
Sort Gate 94.1
cKit (Kit)
CD25 (Il2ra)
B
scRNAseq
UMAP_2
UMAP_1
Thy
ATO
ATO
Thy
C
ATO
Thy
ETP
DN2a
DN3
DN2b
UMAP_3
UMAP_1
D
early
intermediate
late
UMAP_3
UMAP_1
E
Il2ra
Bcl11b
Lef1
UMAP3
UMAP_3
UMAP1
F
Early Clusters (9,4,2,6,7)
Intermediate Clusters (5,3,0,1)
Late Clusters (1,8,11)
Thy
ATO
Xist
Rps27rt
Rpl38
Dntt
Ifitm1
Ly6d
Hmgn2
Rpl23a-ps3
Fcer1g
Gzma
Malat1
Nkg7
Ifitm2

Fig. S2. Gene expression profiles of BM-derived early pro-T cells in vitro recapitulate those of *in vivo* thymic early pro-T cells, on single-cell level.

(A) Illustration of sample purification procedures and FACS sorting strategies for the scRNA-seq experiments, comparing *in vivo* and *in vitro* derived early pro-T cells' single-cell expression profiles. *(B)* Aligned *in vivo* and *in vitro* derived scRNA-seq profiles after CCA scaling, shown in UMAP1-2. The integrated data contains 6167 cells from ATO, and 4783 cells from thymus, 10950 cells total. *(C-F)* Analysis of cell cycle-regressed integrated data, shown in UMAP 1-3 for the clearest separation of developmental stages. *(C)* Cells colored by origin of sample, i.e. 'Thy' for *in vivo* thymocytes and 'ATO' for pro-T cells derived from ATO-DLL4 as discussed in A). Trajectory annotated based on expression of stage marker genes. *(D)* Cells colored with clustering assignment of integrated data. Clustering was performed with Louvain clustering algorithm on PC1-20 of integrated data. *(E)* T- developmental marker genes expression pattern. *(F)* Within the early, middle and late developmental sub-clusters, the average gene expression level (size and log normalized transcript count data) comparison between thymic pro-T cells (Thy) and the *in vitro* derived pro-T cells (ATO). Off-diagonal outlier genes were labeled. Note that the 'Thy' data were obtained from female mice whereas the 'ATO' data were derived from LSKs of male mice, hence the Xist expression in 'Thy' data only.

Figure S3

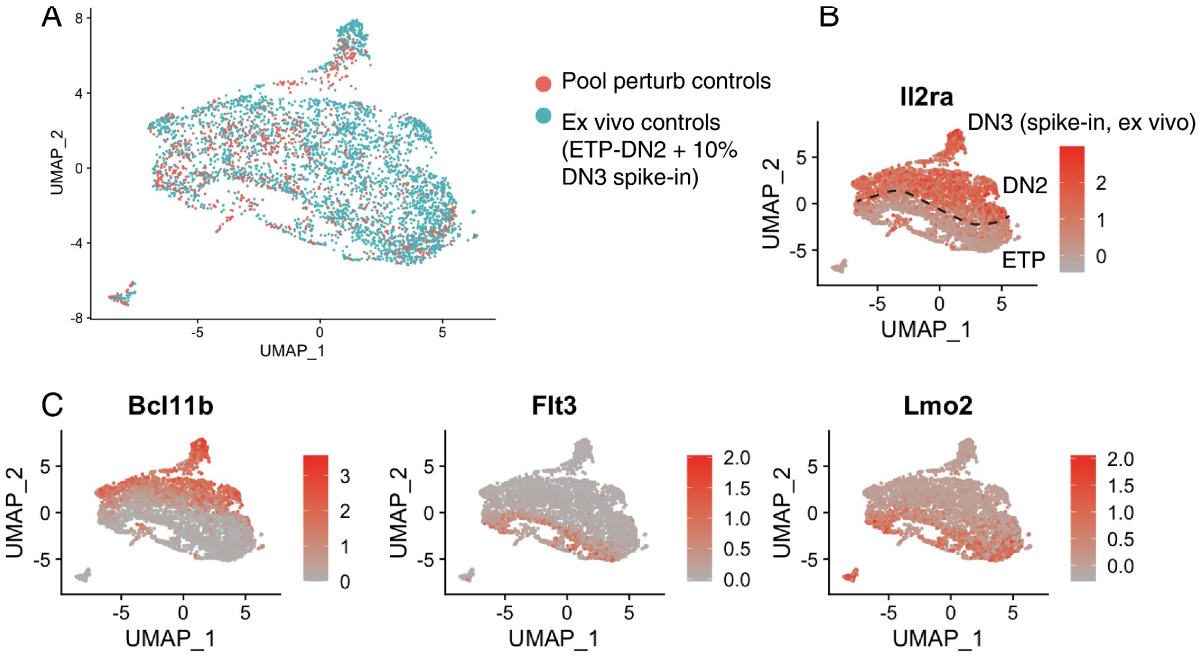

Fig. S3. Alignment of Cas9;Bcl2-transgenic control cells developing in vitro with wildtype non-transgenic B6 thymic pro-T cells developing in vivo.

(A) Comparison of control samples from the present Phase 1 pool-perturbation study with scRNA-seq data for normal, unperturbed, wildtype B6 thymic pro-T cells from ref. (*11*). B6 thymic pro-T cells included Kit^{high} DN1 (ETP)-DN2 cells from thymus plus a spike-in of 10% DN3 cells from thymus to identify developmental direction unequivocally (Accession number GSE137165). Samples were aligned by CCA for display on UMAP1-2. *(B)* Expression of *Il2ra* (encoding CD25) shows the ETP/DN2a border of the pooled distribution. *(C)* Expression of developmental marker genes shows the developmental identities of the cells in the region of full intermixing. *Bcl11b*: commitment. *Flt3, Lmo2*: earliest ETPs. Note that due to the limited in vitro developmental time, control samples from this study were just initiating commitment and did not progress as far as the DN3 spike-in cells in the in vivo sample.

Fig. S4

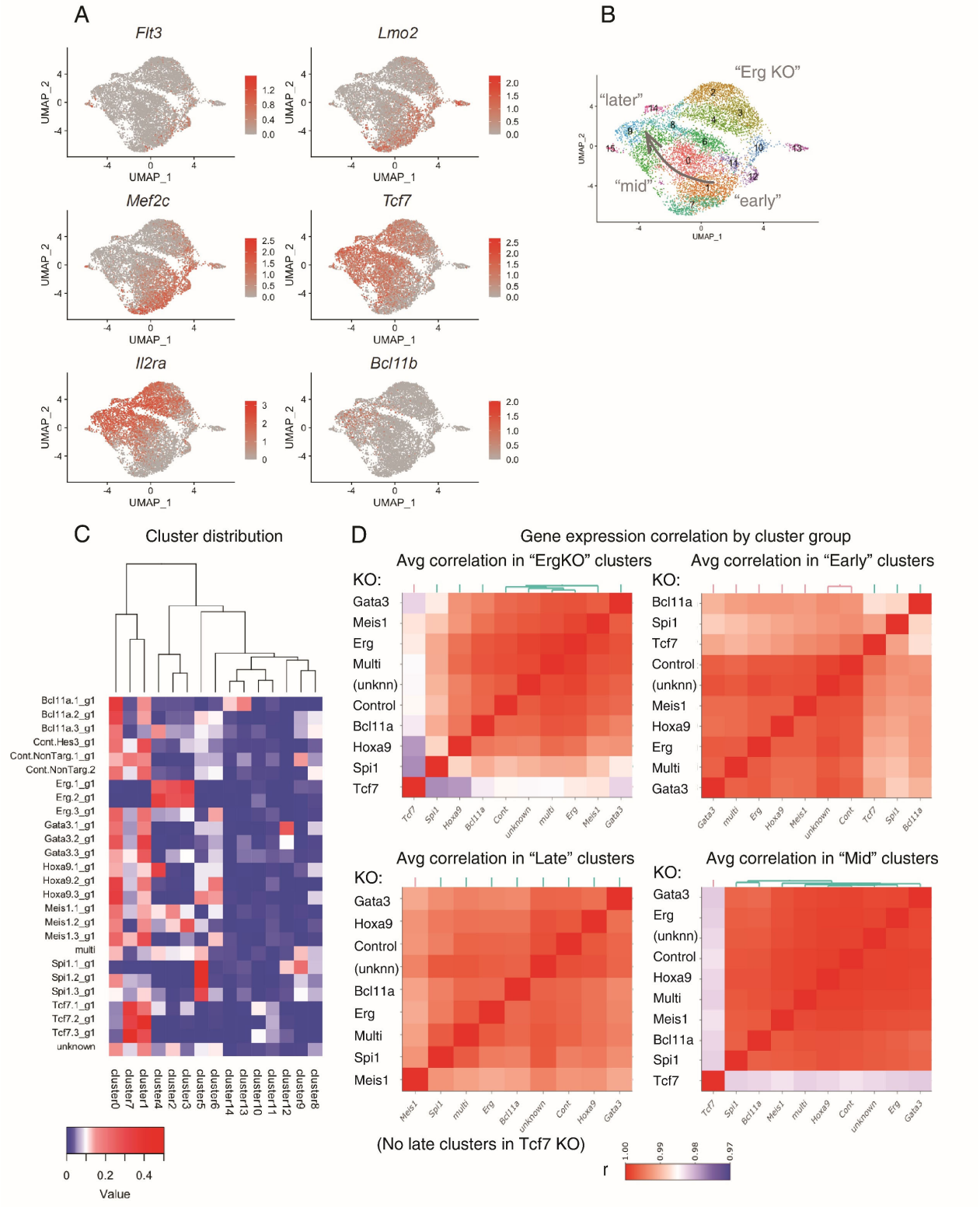
A
Flt3
Lmo2
Mef2c
Tcf7
Il2ra
Bcl11b
UMAP_1
UMAP_2
B
"Erg KO"
"later"
"mid"
"early"
C
Cluster distribution
Bcl11a.1_g1
Bcl11a.2_g1
Bcl11a.3_g1
Cont.Hes3_g1
Cont.NonTarg.1_g1
Cont.NonTarg.2
Erg.1_g1
Erg.2_g1
Erg.3_g1
Gata3.1_g1
Gata3.2_g1
Gata3.3_g1
Hoxa9.1_g1
Hoxa9.2_g1
Hoxa9.3_g1
Meis1.1_g1
Meis1.2_g1
Meis1.3_g1
multi
Spi1.1_g1
Spi1.2_g1
Spi1.3_g1
Tcf7.1_g1
Tcf7.2_g1
Tcf7.3_g1
unknown
cluster0
cluster7
cluster1
cluster4
cluster2
cluster3
cluster5
cluster6
cluster14
cluster13
cluster10
cluster11
cluster12
cluster9
cluster8
Value
D
Gene expression correlation by cluster group
Avg correlation in "ErgKO" clusters
Avg correlation in "Early" clusters
Avg correlation in "Late" clusters
Avg correlation in "Mid" clusters
KO:
(No late clusters in Tcf7 KO)
r

Fig. S4. Knockout effects on cluster distributions of cells relative to normal developmental trajectory.

(A) UMAP1-2 plots of whole pool-perturbation ensemble with cells highlighted based on expression of major T-cell developmental landmark genes. *Flt3, Lmo2, Mef2c*: progenitor-associated genes. *Tcf7*: onset at earliest T-cell specification. *Il2ra*: onset is ETP to DN2a transition marker. *Bcl11b*: activated only during T-lineage commitment, in DN2a to DN2b transition. *(B)* UMAP1-2 plot of combined data showing main trajectory (arrow) and regions of plot containing cells annotated as 'early', 'mid', 'late', and 'Erg KO'. Small numbers denoting clusters are repeated from Fig. 2A. *(C)* Low dimensional representations and clustering assignments mostly represent the differences between genotypes (KOs). Heatmap of cluster distributions resulting from each individual dual gRNA perturbation. Color scale shows fractions of cells in each cluster. Results show a general agreement of cluster distributions of perturbations against the same genes, with a few exceptions, such as Erg.3 (3rd pair of gRNAs targeting Erg). Raw cluster distributions for each gRNA are shown in Table S12. *(D)* Heatmaps showing Pearson r values for correlation between average gene expression patterns in different perturbations, where the cells fall within the shared 'common clusters'. Comparison of gene expression patterns among cells in different samples within the same cluster approximates comparison of gene expression among cells in different samples at the same pseudotime values. The 4 'common clusters' were defined as: 'early clusters': 7, 1, 11; 'mid clusters': 0, 6; 'late clusters': 9, 5, 8; 'Erg KO clusters': 4, 3, 2, representing regions of the UMAP manifold shown in panel *(B)*; these sub-clusters are defined in Fig. 2A. KO identities are listed in the same order from the bottom to top and from left to right; (unknn)=unknown (cells with gRNA identity indeterminate). Note that the color scale of heatmap represents Pearson r of 0.97 to 1. This implies that within the same 'common clusters', the expression profiles between KOs and Cont were very similar, with the exception of Tcf7 KO in the 'mid' and 'Erg KO' clusters. Note that Tcf7 KO cells were not found in 'late clusters'.

Fig. S5

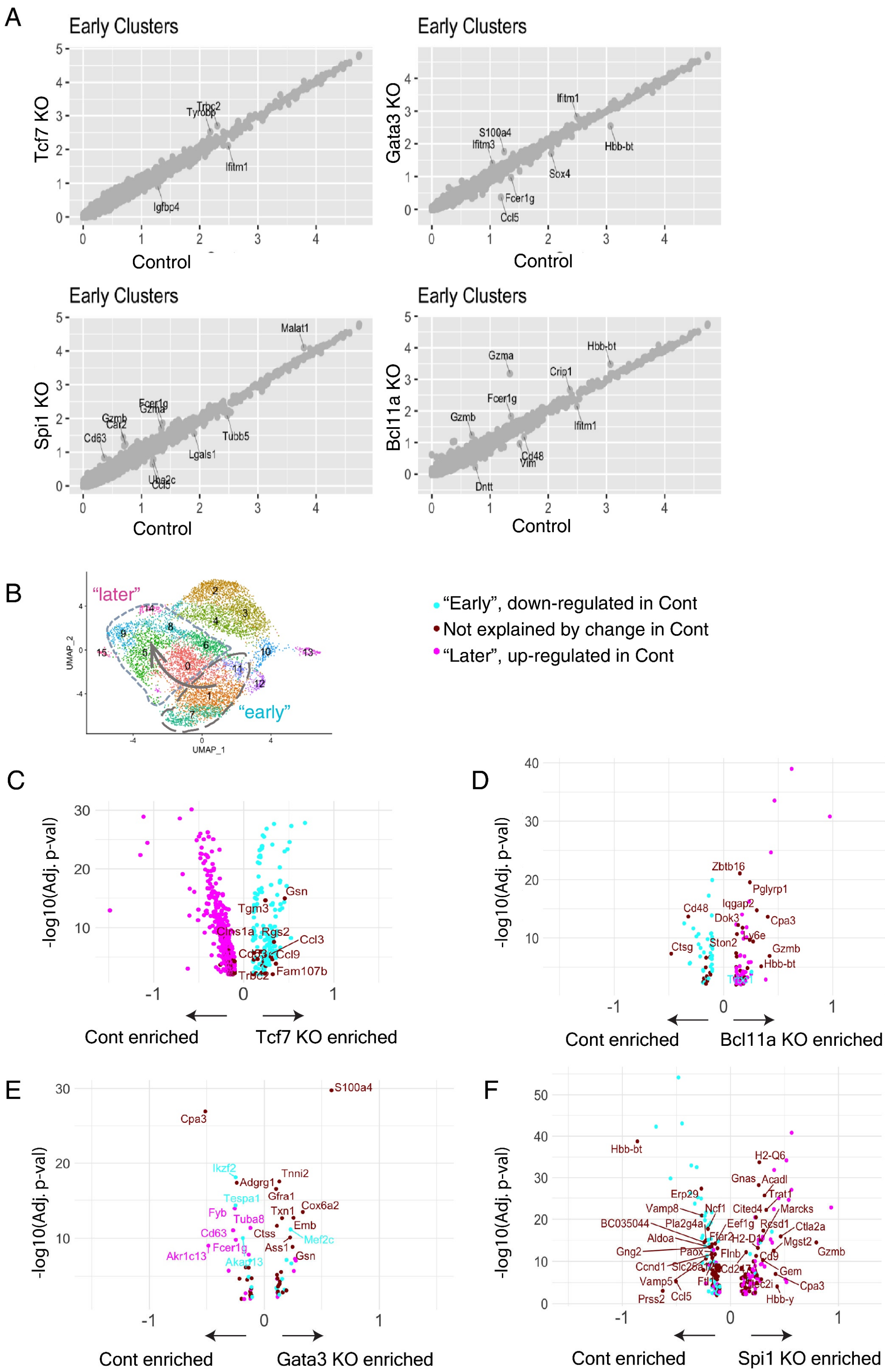

A
Early Clusters
Tcf7 KO
Control
Trbc2
Tyrobp
Ifitm1
Igfbp4
Early Clusters
Gata3 KO
Control
Ifitm1
S100a4
Ifitm3
Hbb-bt
Sox4
Fcer1g
Ccl5
Early Clusters
Spi1 KO
Control
Malat1
Fcer1g
Gzma
Gzmb
Car2
Cd63
Tubb5
Lgals1
Early Clusters
Bcl11a KO
Control
Hbb-bt
Gzma
Crip1
Fcer1g
Gzmb
Ifitm1
Cd48
Vim
Dntt
B
"later"
"early"
UMAP_1
UMAP_2
"Early", down-regulated in Cont
Not explained by change in Cont
"Later", up-regulated in Cont
C
-log10(Adj. p-val)
Gsn
Tgm3
Rgs2
Ccl3
Ccl9
Fam107b
Cont enriched
Tcf7 KO enriched
D
-log10(Adj. p-val)
Zbtb16
Pglyrp1
Iqgap2
Cd48
Dok3
Cpa3
Ly6e
Ston2
Ctsg
Gzmb
Hbb-bt
Cont enriched
Bcl11a KO enriched
E
-log10(Adj. p-val)
S100a4
Cpa3
Ikzf2
Tnni2
Adgrg1
Gfra1
Tespa1
Cox6a2
Fyb
Txn1
Tuba8
Emb
Cd63
Ctss
Mef2c
Fcer1g
Ass1
Akr1c13
Gsn
Cont enriched
Gata3 KO enriched
F
-log10(Adj. p-val)
Hbb-bt
H2-Q6
Gnas
Acadl
Erp29
Trat1
Vamp8
Ncf1
Cited4
Marcks
BC035044
Pla2g4a
Eef1g
Rcsd1
Ctla2a
Aldoa
H2-DMa
Mgst2
Gng2
Paox
Flnb
Cd9
Gzmb
Ccnd1
Gem
Vamp5
Cpa3
Prss2
Ccl5
Hbb-y
Cont enriched
Spi1 KO enriched

Fig. S5. Relationship of knockout effects to gene expression changes occurring naturally with T-cell lineage developmental progression.

(A) Scatterplots comparing average gene expression levels [ln(count+1)] between KOs and Control (Cont) cells within the shared 'early' common clusters only (see Fig. S4B; sub-clusters 7,1,11 as defined in Fig. 2A). Only the rare genes off diagonal are annotated. Note high similarity of gene expression levels between KOs and Cont in these same 'common clusters'. *(B)-(F)* Dissection of KO effects on developmental "speed" (cf. Fig. 3B): relationship of genes differentially regulated in each KO to genes normally changing expression in development *(B)* Clusters used to define individual genes as being expressed "early" or "late" along the canonical pathway. UMAP1-2 illustration of the clusters pooled and contrasted for the differential expression test performed on Control (Cont) cells only across these clusters, to define genes that change during the early to late transition under normal developmental conditions (i.e., no perturbation). (*C-F)* Volcano plots showing the differentially expressed genes between Cont and individual KOs (x axes), comparing this effect with their expression change in normal development. The color of dots distinguishes genes that also increased (magenta) or decreased (cyan) expression within Cont cells, during their normal developmental progression from 'early clusters' to 'mid' and 'late' clusters, as annotated in *(B)*. Genes that were differentially expressed between KOs and Cont but were not differentially regulated in this normal developmental transition are labeled as dark brick red. Concordance of color labels with positive or negative values along the x axis helps to visualize whether the differential gene expression between WT and KOs was merely reflecting a developmental acceleration or a stalled progression. *(C)* Tcf7 KO effects. *(D)* Bcl11a KO effects. *(E)* Gata3 KO effects. *(F)* Spi1 KO effects.

Figure S6

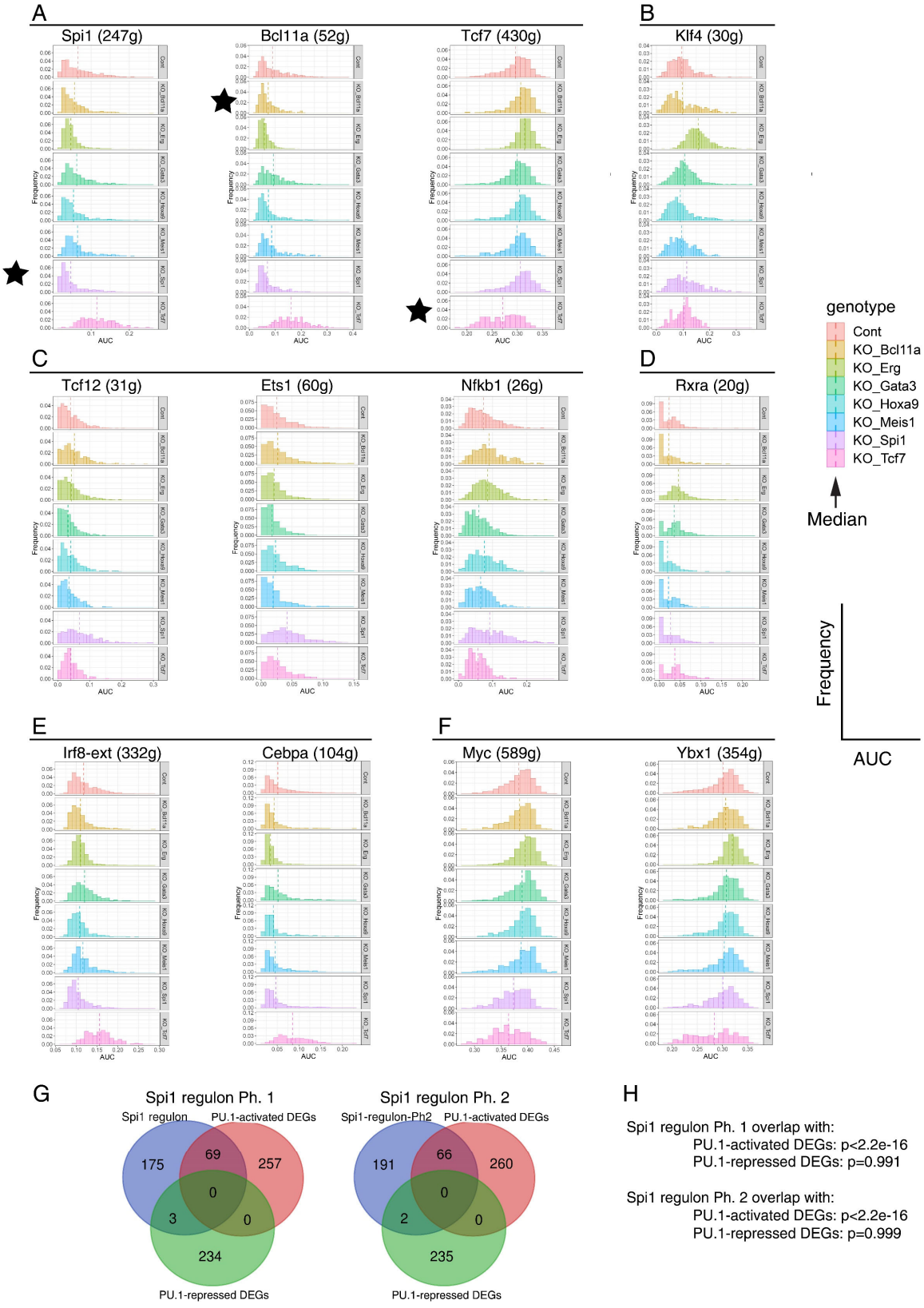
A
Spi1 (247g)
Bcl11a (52g)
Tcf7 (430g)
B
Klf4 (30g)
C
Tcf12 (31g)
Ets1 (60g)
Nfkb1 (26g)
D
Rxra (20g)
E
Irf8-ext (332g)
Cebpa (104g)
F
Myc (589g)
Ybx1 (354g)
Frequency
AUC
genotype
Cont
KO_Bcl11a
KO_Erg
KO_Gata3
KO_Hoxa9
KO_Meis1
KO_Spi1
KO_Tcf7
Median
Frequency
AUC
G
Spi1 regulon Ph. 1
Spi1 regulon
PU.1-activated DEGs
175
69
257
0
3
0
234
PU.1-repressed DEGs
Spi1 regulon Ph. 2
Spi1-regulon-Ph2
PU.1-activated DEGs
191
66
260
0
2
0
235
PU.1-repressed DEGs
H
Spi1 regulon Ph. 1 overlap with:
PU.1-activated DEGs: p<2.2e-16
PU.1-repressed DEGs: p=0.991
Spi1 regulon Ph. 2 overlap with:
PU.1-activated DEGs: p<2.2e-16
PU.1-repressed DEGs: p=0.999

Fig. S6. Inferred TF activities and regulatory connections by SCENIC: histograms of individual representative regulons in the 8 CRISPR pool-perturbation genotypes.

SCENIC analysis was performed on subsets of Cont and individual KOs. *(A)-(F)* Histograms of frequencies of cells with a given Area Under the Curve (AUC) of activity of the indicated regulon, among cells of a given genotype (perturbation state) within the pool-perturbation scRNA-seq ensemble. Vertical dashed lines indicate medians. Key to panels *(A-F)* is on right of figure; values are given in Table S4A. *(A)* Regulons corresponding to factors directly targeted among the perturbation conditions, indicated by black stars. *(B)* Klf4 regulon, specifically upregulated when Erg is removed. *(C)* Regulons specifically upregulated in normal cells progressing along the T-cell developmental pathway. Note that all are specifically upregulated when Spi1 is removed. *(D)* Rxra regulon, rarely expressed but specifically upregulated in Erg KO cells. *(E)* Myeloid-associated regulons for Irf family transcription factors and Cebpa: Note strong upregulation in absence of Tcf7 and possibly in absence of Gata3 as well. *(F)* Cell blastogenesis and proliferation-associated regulons, for Myc and Ybx1. Note upshift in Erg KO and downshift in Tcf7 KO. Analysis details are given in Methods. For full quantitation of all scorable regulons in the dataset, see Table S4. *(G)* Overlap of Spi1 (PU.1) regulon members with highly validated PU.1-activated and PU.1-repressed DEGs, defined by sensitive bulk RNA-seq of both gain and loss of function perturbations (*43*). Both the Spi1 regulon members defined in Phase 1 pool-perturb samples (Table S4) and the Spi1 regulon members defined in the later, Bcl11b KO vs. WT samples (Table S8) are compared with these DEGs. Gene lists for the overlap sets are given in Table S9A. (H) Fisher's exact test p values for overlaps between Spi1 regulon members and functionally validated PU.1 (*Spi1* gene product) DEGs (shown in *(G)*); calculated estimating maximum detectable number of expressed genes from the scRNA-seq dataset to be 7000.

Fig. S7

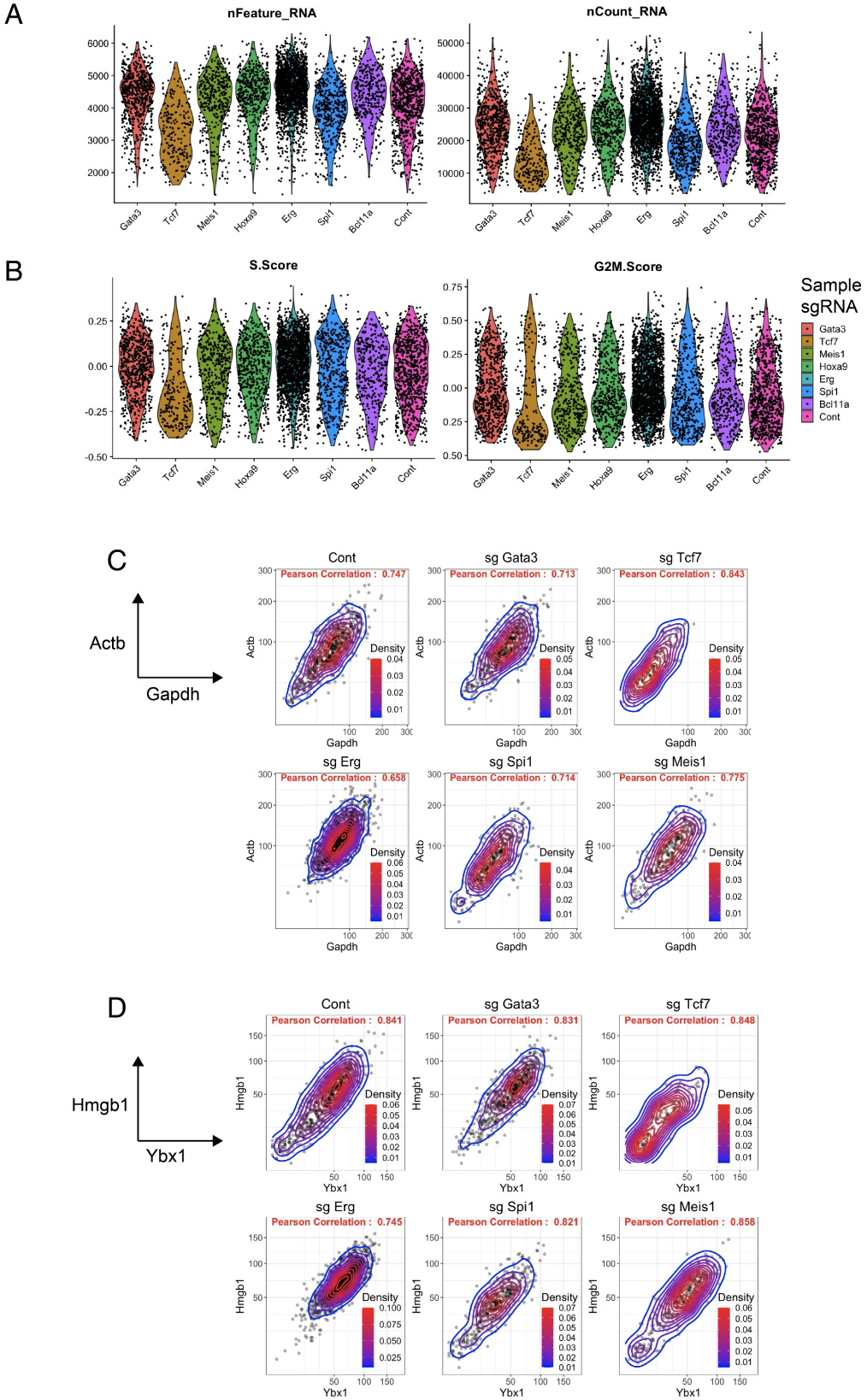
A
nFeature_RNA
nCount_RNA
Gata3
Tcf7
Meis1
Hoxa9
Erg
Spi1
Bcl11a
Cont
B
S.Score
G2M.Score
Sample
sgRNA
C
Cont
sg Gata3
sg Tcf7
sg Erg
sg Spi1
sg Meis1
Actb
Gapdh
Pearson Correlation : 0.747
Pearson Correlation : 0.713
Pearson Correlation : 0.843
Pearson Correlation : 0.658
Pearson Correlation : 0.714
Pearson Correlation : 0.775
Density
D
Hmgb1
Ybx1
Pearson Correlation : 0.841
Pearson Correlation : 0.831
Pearson Correlation : 0.848
Pearson Correlation : 0.745
Pearson Correlation : 0.821
Pearson Correlation : 0.858

Fig. S7. Transcription factor knockout impacts on cell biological parameters of developing pro-T cells.

(A) Distributions of number of genes detected, number of transcripts detected, and *(B)* inferred cell cycle stages, in subsets of the pool-perturbation ensemble separated according to genes perturbed. *(C)-(D)* Scatterplots of transcript distributions of housekeeping genes *(C)* and cell cycle-associated genes *(D)*, separated by genes perturbed. Number of cells of each KO in analysis: Cont: 793, Bcl11a: 353, Erg: 1397, Gata3: 686, Hoxa9: 503, Meis1: 409, Spi1: 481, Tcf7: 215.

Fig. S8

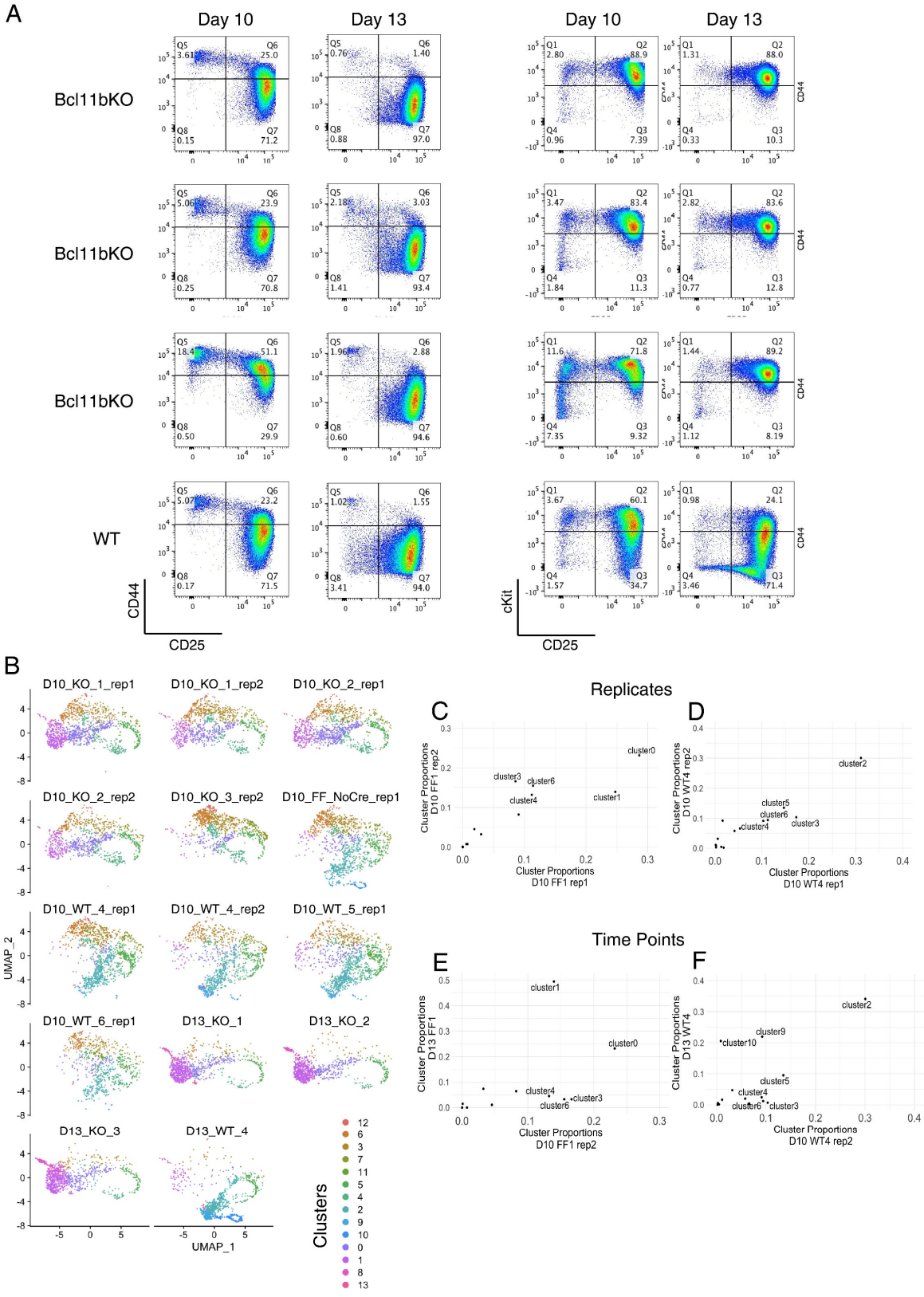
A
Day 10
Day 13
Day 10
Day 13
Bcl11bKO
Bcl11bKO
Bcl11bKO
WT
CD44
CD25
cKit
CD25
B
D10_KO_1_rep1
D10_KO_1_rep2
D10_KO_2_rep1
D10_KO_2_rep2
D10_KO_3_rep2
D10_FF_NoCre_rep1
D10_WT_4_rep1
D10_WT_4_rep2
D10_WT_5_rep1
D10_WT_6_rep1
D13_KO_1
D13_KO_2
D13_KO_3
D13_WT_4
UMAP_2
UMAP_1
Clusters
12
6
3
7
11
5
4
2
9
10
0
1
8
13
Replicates
C
Cluster Proportions D10 FF1 rep2
Cluster Proportions D10 FF1 rep1
D
Cluster Proportions D10 WT4 rep2
Cluster Proportions D10 WT4 rep1
Time Points
E
Cluster Proportions D13 FF1
Cluster Proportions D10 FF1 rep2
F
Cluster Proportions D13 WT4
Cluster Proportions D10 WT4 rep2

Fig. S8. Surface marker and transcriptome profiles of WT and Bcl11b KO single-cell samples.

(*A)* Flow cytometry profiles of WT and Bcl11b KO cells collected from ATO-DLL4 culture system at D10 and D13 of culture. Note that the *Bcl11b* locus is starting to be transcribed in normal DN2A cells around D7, so that D10 represents ~3 days later, D13 represents ~6 days later. CD25 staining from the indicated samples is shown correlated with CD44 and c-Kit (cKit in figure) staining. Downregulation of CD44 (left panels) and c-Kit(right panels) normally marks DN2 to DN3 progression. Data show that compared to WT control, the cells missing Bcl11b could still similarly turn off CD44 but failed to downregulate c-Kit expression levels. *(B)* UMAP 1-2 display of the integrated scRNA-seq data, separated by individual samples. All animals, including WT controls, were Cre^{+} except for one D10 $Bcl11b^{fl/fl}$ animal, which serves as an additional no-Cre control. All other $Bcl11b^{fl/fl}$ ("FF") animals were Cre^{+} and are thus considered Bcl11b KO. Cell numbers in subpanels: 'D10_FF_1_rep1': 1366, 'D10_FF_1_rep2': 1083, 'D10_FF_2_rep1': 1261, 'D10_FF_2_rep2': 1038, 'D10_FF_3_rep2': 1115, 'D10_FF_NoCre_rep1': 1300, 'D10_WT_4_rep1': 1352, 'D10_WT_4_rep2': 1075, 'D10_WT_5_rep1': 1377, 'D10_WT_6_rep1': 795, 'D13_FF_1': 1017, 'D13_FF_2' : 1061, 'D13_FF_3': 1022, D13_WT_4: 1147. *(C)-(D)* Cluster distributions (shown in proportions), comparing different biological replicates of cells derived from BM of the same animal origin. This shows replicability of *ex-vivo* derivation and scRNA-seq experimental setups. R=0.89 for C, R=0.94 for D. *(E)-(F)* Cluster distributions comparing samples harvested from D13 (y axis) with those harvested from D10 (x axis) of the same animal origins. WT: R=0.66, FF: R=0.54. Cluster assignment is the same as described in Fig. 6D.

Figure S9

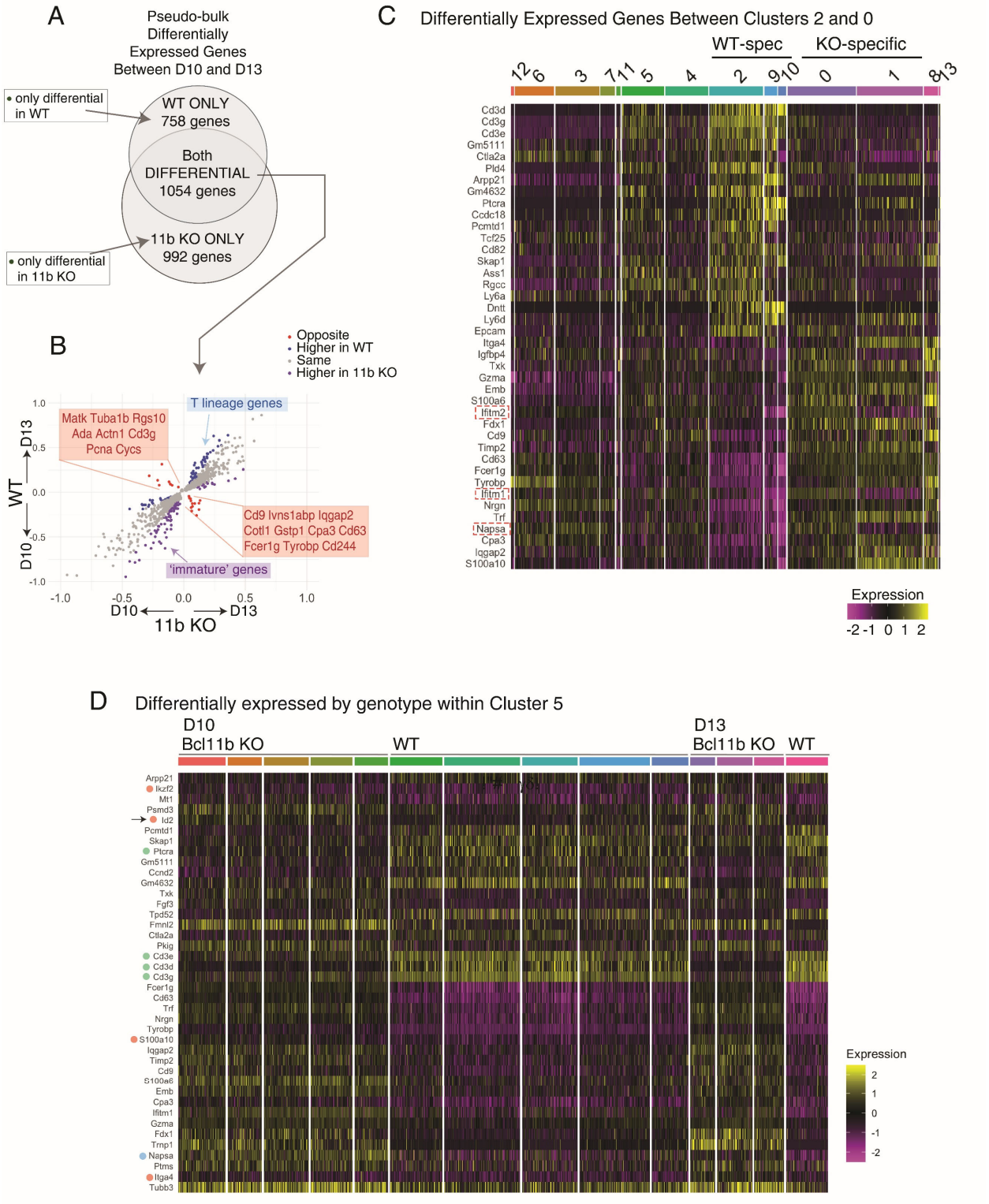
A
Pseudo-bulk Differentially Expressed Genes Between D10 and D13
• only differential in WT
WT ONLY 758 genes
Both DIFFERENTIAL 1054 genes
11b KO ONLY 992 genes
• only differential in 11b KO
B
Opposite
Higher in WT
Same
Higher in 11b KO
T lineage genes
Matk Tuba1b Rgs10 Ada Actn1 Cd3g Pcna Cycs
Cd9 Ivns1abp Iqgap2 Cotl1 Gstp1 Cpa3 Cd63 Fcer1g Tyrobp Cd244
'immature' genes
WT
D13
D10
11b KO
C
Differentially Expressed Genes Between Clusters 2 and 0
WT-spec
KO-specific
Expression
D
Differentially expressed by genotype within Cluster 5
D10 Bcl11b KO
WT
D13 Bcl11b KO
WT
Expression

Fig. S9. Time-dependent gene expression deviations between Bcl11b KO and WT late pro-T cells.

(*A)* Venn diagram showing the numbers of genes with changing expression from D10 to D13 and their overlaps between the two genotypes. These genes are listed in Table S6. Differential expression comparison was made between genes in cells that were harvested on D10 and D13, separately analyzed in WT and Bcl11b KO, and the Venn diagram shows the intersection between these two DEG sets. Differential expression tests were performed with a generalized linear model with Quasi-Poisson distribution of transcript count using Monocle3. Statistical significance was calculated by Wald test, and adjusted p-values represent false discovery rate. The differentially expressed genes were defined based on adj.p-val < 1E-10 for Bcl11b KO and adj.p-val < 1E-5 for WT, accounting for the cell number difference. WT: N= 5899 cells from D10 and 1147 cells from D13. Bcl11b KO: N= 5863 cells from D10 and 3100 cells from D13.

(*B)* Scatterplot comparing genes that were differentially regulated in both the WT and Bcl11b KO pseudo-bulk measurements, showing whether the directions of expression change over time were the same or opposite in the two genotypes. Shown are the 1054 genes that were significantly differentially expressed in both of the genotypes. Axes represent “log fold changes” of Seurat-processed expression with respect to time in each genotype. Red dots: genes that changed expression in opposite directions between WT and Bcl11b KO; cyan dots: genes expressed more highly in WT at both timepoints (≥1.7 fold difference in ‘estimates’, and the ‘estimate’ in at least one of the genotype ≥0.1); blue-purple dots: genes with sustained higher expression in Bcl11b KO (≥1.7 fold difference in ‘estimates’, and the ‘estimate’ in at least one of the genotype ≥ 0.1).

(C) Heatmap showing the top 20 differentially expressed genes between cluster 0 and cluster 2, in both directions, also see Table S7A. (Wilcoxon Rank Sum test, filtered by minimally expressed by 25% cells in of one of the clusters, and adjusted p-val < 1e-50).
(D) Heatmap of differentially expressed genes between WT and Bcl11b KO in only the cells from cluster 5, revealing the gene expression differences that caused the separation

shown in Fig. 6F. (Wilcoxon Rank Sum test, filtered by minimally expressed by 25% cells in of one of the clusters, and adjusted p-val < 1E-20, top and bottom 20 genes ranked by average log expression differences (‘avg_logFC’ in Seurat) are displayed, calculated using Seurat 3. Full DE analysis see Table S7B.) Red dots: genes that are enriched in Bcl11b KO compared to WT within cluster 5 only, more markedly expressed in D13 than D10. Green dots: T-lineage progression genes, higher in WT. N=762 cells from Bcl11b KO in cluster 5 and N=868 cells from WT in cluster 5.

Figure S10

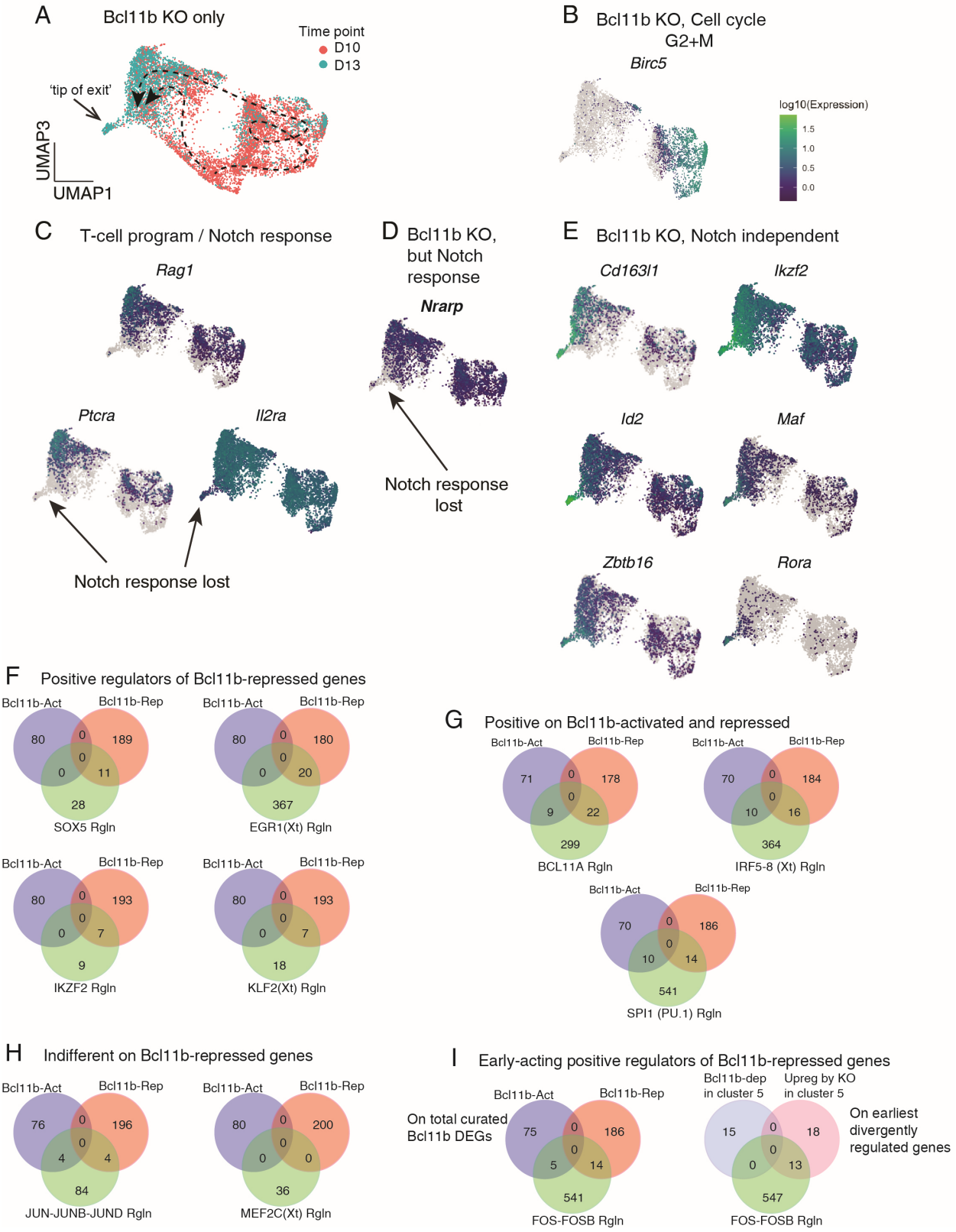
A
Bcl11b KO only
Time point
D10
D13
'tip of exit'
UMAP3
UMAP1
B
Bcl11b KO, Cell cycle G2+M
Birc5
log10(Expression)
1.5
1.0
0.5
0.0
C
T-cell program / Notch response
Rag1
Ptcra
Il2ra
Notch response lost
D
Bcl11b KO, but Notch response
Nrarp
Notch response lost
E
Bcl11b KO, Notch independent
Cd163l1
Ikzf2
Id2
Maf
Zbtb16
Rora
F
Positive regulators of Bcl11b-repressed genes
Bcl11b-Act
Bcl11b-Rep
80
0
189
0
0
11
28
SOX5 Rgln
80
0
180
0
0
20
367
EGR1(Xt) Rgln
80
0
193
0
0
7
9
IKZF2 Rgln
80
0
193
0
0
7
18
KLF2(Xt) Rgln
G
Positive on Bcl11b-activated and repressed
71
0
178
0
9
22
299
BCL11A Rgln
70
0
184
0
10
16
364
IRF5-8 (Xt) Rgln
70
0
186
0
10
14
541
SPI1 (PU.1) Rgln
H
Indifferent on Bcl11b-repressed genes
76
0
196
0
4
4
84
JUN-JUNB-JUND Rgln
80
0
200
0
0
0
36
MEF2C(Xt) Rgln
I
Early-acting positive regulators of Bcl11b-repressed genes
On total curated Bcl11b DEGs
75
0
186
0
5
14
541
FOS-FOSB Rgln
Bcl11b-dep in cluster 5
Upreg by KO in cluster 5
15
0
18
0
0
13
547
FOS-FOSB Rgln
On earliest divergently regulated genes

Fig. S10. Fine-grained examination of the Bcl11b KO trajectory.

(A) UMAP 1 vs. UMAP 3 plot of only the cells derived from Bcl11b KO animals from both experiments, at D10 (red) and D13 (blue) timepoints. Bcl11b KO cells were first subsetted from the ensemble (Fig. 5C,D) by the hashtag assignments, excluding a small, shared non-T cluster that is also present in Bcl11b KO and WT, and then used to generate these UMAP plots (N=8899 cells). Cells colored by time point of sample collection, D10 (red) and D13 (blue), showing Bcl11b KO samples' distribution changes with respect to time, on UMAP1-3. 'Tip of exit' corresponds to cluster 8 in Fig. 5C, the cells with the most extreme Bcl11b KO phenotype. Central gap in pattern: cells with Bcl11b KO genotype from D10-specific clusters representing stages before the normal time of Bcl11b expression were included to compute UMAP layout, but are masked out from these displays to focus on changes in transcriptome distributions at later stages. Dashed lines indicate approximate trajectories for the Bcl11b KO cells (upper path with more proliferation, lower path with less proliferation). *(B)-(E)* Selected genes' expression patterns on the UMAP 1-3 plot of Bcl11b KO cells only. N=6820 cells. *(B)* Expression of *Birc5* as marker for cycling G2+M cells. *(C)* The expression of Notch response genes within the post-commitment T-cell program, *Ptcra* and *Il2ra*, and E protein-regulated *Rag1*: all are downregulated at the bottom left 'tip' of this UMAP 1-3 display. *(D) Nrarp*, a rare Notch-dependent gene that is actually upregulated in Bcl11b KO populations overall, also loses expression in cells at the bottom left 'tip'. This confirms that Notch signaling itself, not only WT DN3-associated genes, is turned off in cells at the 'tip'. *(E)* Notch-independent genes associated with innate lymphoid cells, TCR$\gamma\delta$ cells, and agonist-selected TCR$\alpha\beta$ T cells undergoing intrathymic stimulation: all show increased expression in D13 cells (left-hand half of UMAP1-3 plot) with maximal expression at bottom left 'tip'.

(F)-(H) Assessment of candidate drivers of the Bcl11b-repressed program: representation of individual members of different Bcl11b KO-enriched regulons among highly curated Bcl11b-activated and Bcl11b-repressed DEGs from bulk RNA-seq (*37*). For gene names and p values of regulon overlaps with Bcl11b-repressed targets, see Table S9B. *(F)* Regulons with strongly preferential member overlap with Bcl11b-repressed DEGs. *(G)*

Regulons with significant member overlaps with both Bcl11b-activated and Bcl11b-repressed DEGs. *(H)* Regulons with no significant member preference in overlap with DEGs. *(I)* Comparison of overlaps of Fos-FosB regulons with total curated Bcl11b-regulated DEGs (left) or with genes that indicate the first divergence between Bcl11b KO and WT, within cluster 5 (right). Lists of KO-specific and WT-specific genes in cluster 5 were taken from Fig. S9D and Table S7B. Fos, FosB regulon overlap with total Bcl11b-repressed DEGs, p value = 0.739 (see Table S9B); Fos, Fosb regulon overlap with these KO-specifically upregulated genes within cluster 5, p value = 2.5e-07 (Fisher's exact test).

Figure S11

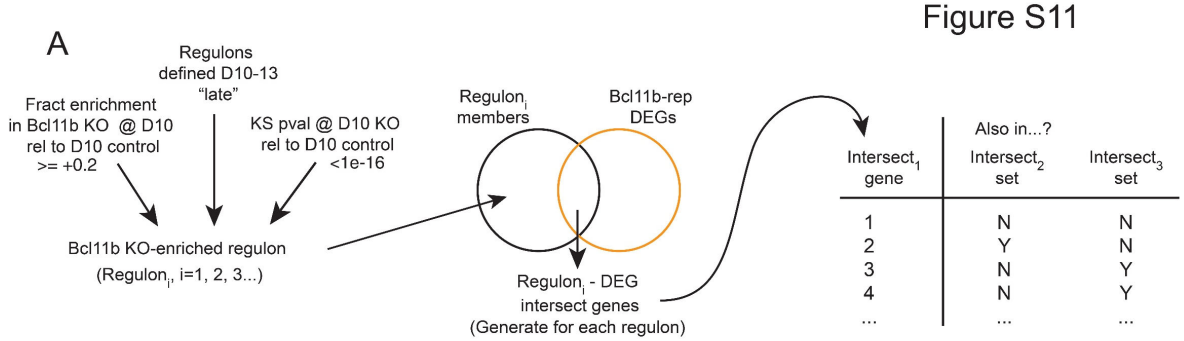
A
Regulons defined D10-13 "late"
Fract enrichment in Bcl11b KO @ D10 rel to D10 control >= +0.2
KS pval @ D10 KO rel to D10 control <1e-16
Bcl11b KO-enriched regulon (Regulon$_i$, i=1, 2, 3...)
Regulon$_i$ members
Bcl11b-rep DEGs
Regulon$_i$ - DEG intersect genes (Generate for each regulon)
Intersect$_1$ gene
Also in...?
Intersect$_2$ set
Intersect$_3$ set
1 N N
2 Y N
3 N Y
4 N Y
... ...

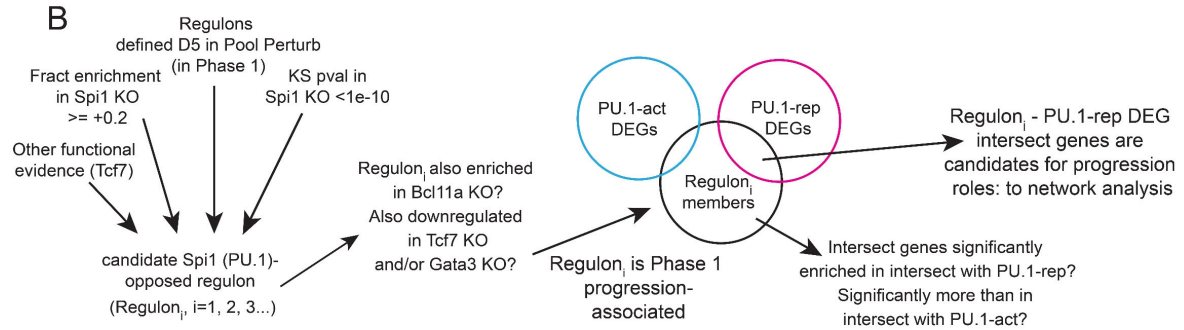
B
Regulons defined D5 in Pool Perturb (in Phase 1)
Fract enrichment in Spi1 KO >= +0.2
KS pval in Spi1 KO <1e-10
Other functional evidence (Tcf7)
candidate Spi1 (PU.1)-opposed regulon (Regulon$_i$, i=1, 2, 3...)
Regulon$_i$ also enriched in Bcl11a KO? Also downregulated in Tcf7 KO and/or Gata3 KO?
PU.1-act DEGs
PU.1-rep DEGs
Regulon$_i$ members
Regulon$_i$ is Phase 1 progression-associated
Regulon$_i$ - PU.1-rep DEG intersect genes are candidates for progression roles: to network analysis
Intersect genes significantly enriched in intersect with PU.1-rep? Significantly more than in intersect with PU.1-act?

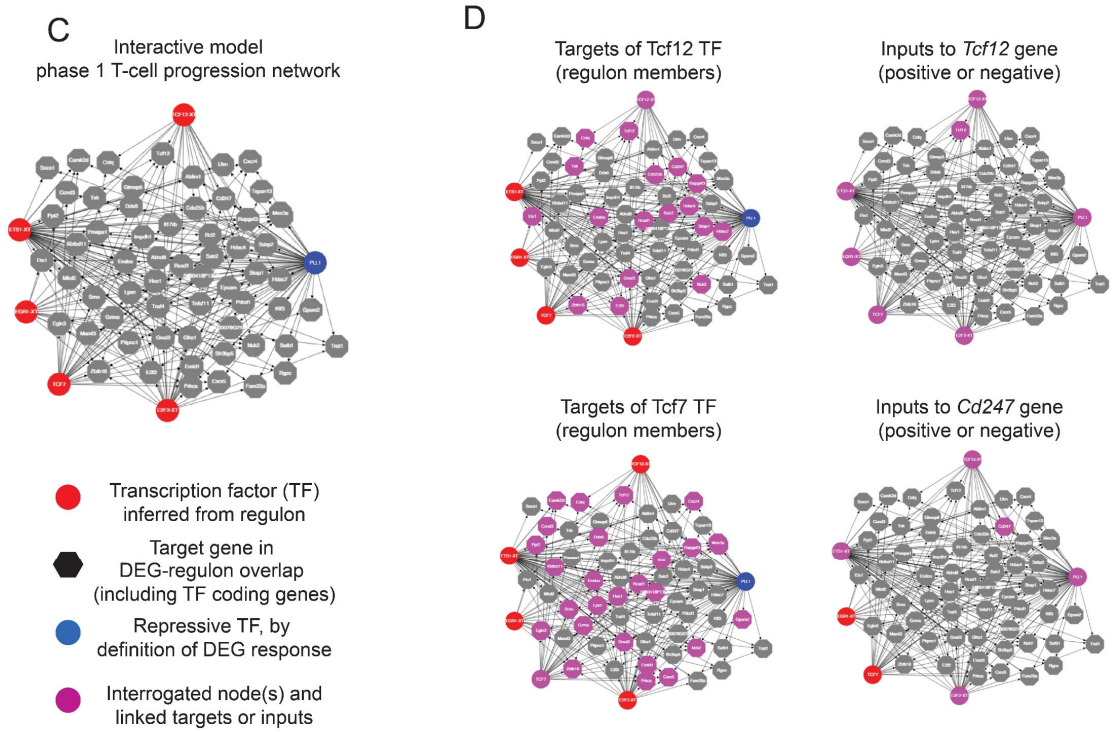
C
Interactive model phase 1 T-cell progression network
Transcription factor (TF) inferred from regulon
Target gene in DEG-regulon overlap (including TF coding genes)
Repressive TF, by definition of DEG response
Interrogated node(s) and linked targets or inputs
D
Targets of Tcf12 TF (regulon members)
Inputs to *Tcf12* gene (positive or negative)
Targets of Tcf7 TF (regulon members)
Inputs to *Cd247* gene (positive or negative)

Fig. S11. Gene network analysis of Phase 1 specification and the Bcl11b knockout substructure.

(A) Flow chart for selection of regulons identified as responding to Bcl11b KO, and overlaps between those regulons and Bcl11b-repressed DEGs. Data and gene lists for input regulons were from Table S8; regulons were selected with fold change score enrichment between Bcl11b KO and WT at D10 >+1.2 (Table 8A, bottom), and KS p value <1e-16 (Table 8D). In addition, the Spi1 regulon (defined in Phase 2, fold change score enrichment >+1.15 at D10, KS p value <1e-16) was also included. DEG lists were taken from ref. (*37*) as described in Methods, including genes that were significantly upregulated in all of three different Bcl11b KO models, and are shown with lists of intersecting regulon genes and statistics in Table S9B.
(B) Flow chart for selection of Phase 1 regulons identified as associated with T-lineage developmental progression based on the criteria shown, based on their restraint by Spi1 (PU.1) activity (fold changes >+1.2 and KS values <1e-10 observed in Spi KO, as shown in Table S4). DEG lists were taken from ref. (*43*) as described in Methods and shown in Table S9A. Gene lists and statistics for genes under inferred PU.1 repression are shown in Table S9D,E. Gene lists for genes in the same regulons that overlap with PU.1-activated DEGs are shown in Table S9F. Questions show the tests that were done with results shown in Table S9D. For notation on Tcf7 regulon, see Table S9D. Once selected, PU.1-repressed DEG-intersecting genes within each of the Spi1 KO-enriched regulons were assessed for possible cross-regulatory network interactions by comparison with their representation in other selected regulons, as shown on the right side of (*A*); matrix of specific gene memberships among regulons is shown in Table S9E.
(C) Interactive model of the Phase 1 gene regulatory network, focusing on the regulon members repressed by PU.1 and within the regulons of Ets1-ext, E2f2-ext, Egr1-ext, Tcf12-ext, and Tcf7 (cf. Venn diagram, Fig. 8C). Screenshot of a neutral configuration is shown from the live model at http://bioinfoweb.caltech.edu/tf_targets/. Positions of nodes were manually adjusted to remove overlaps for clear visualization. Note that the regulon sources represented by TFs, represented by circles, are distinct from the nodes representing the genes that code for those TFs.

(D) Examples of the highlighting of targets of selected regulons (Tcf12-ext, Tcf7), left, and highlighting of the inputs to selected target nodes (*Tcf12*, *Cd247*), right. Note that the Tcf12-ext activity is predicted to provide input into member gene *Tcf12* encoding the regulator itself.

Fig. S12

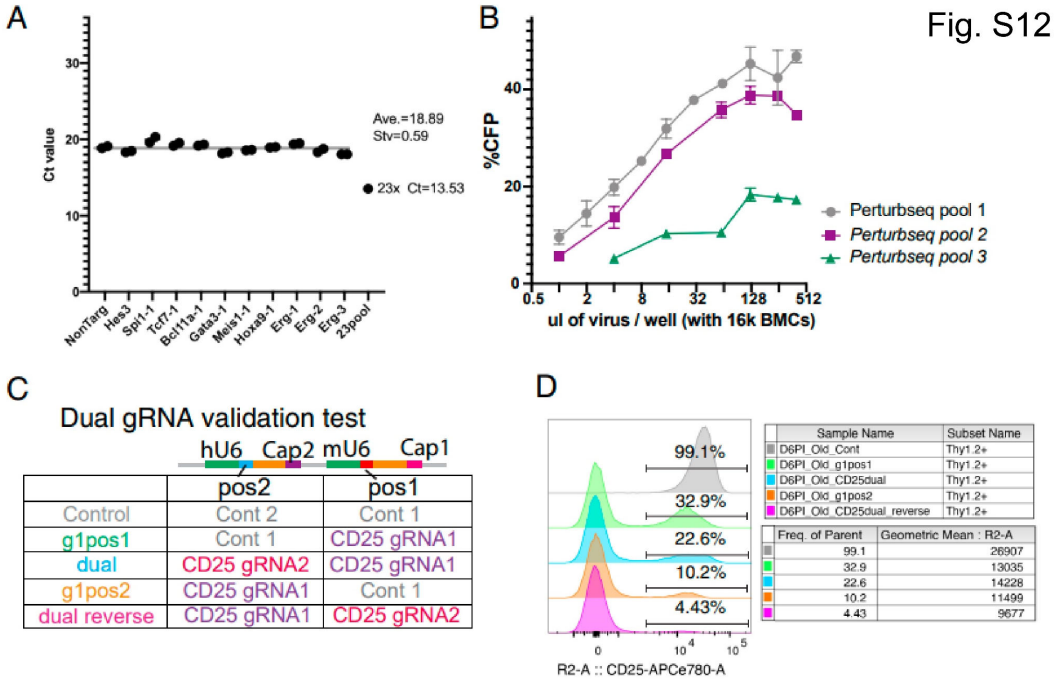
A
Ct value
Ave.=18.89
Stv=0.59
23x Ct=13.53
NonTarg
Hes3
Spi1-1
Tcf7-1
Bcl11a-1
Gata3-1
Meis1-1
Hoxa9-1
Erg-1
Erg-2
Erg-3
23pool
B
%CFP
ul of virus / well (with 16k BMCs)
Perturbseq pool 1
Perturbseq pool 2
Perturbseq pool 3
C
Dual gRNA validation test
hU6 Cap2 mU6 Cap1
pos2
pos1
Control Cont 2 Cont 1
g1pos1 Cont 1 CD25 gRNA1
dual CD25 gRNA2 CD25 gRNA1
g1pos2 CD25 gRNA1 Cont 1
dual reverse CD25 gRNA1 CD25 gRNA2
D
99.1%
32.9%
22.6%
10.2%
4.43%
R2-A :: CD25-APCe780-A
Sample Name
Subset Name
D6PI_Old_Cont
D6PI_Old_g1pos1
D6PI_Old_CD25dual
D6PI_Old_g1pos2
D6PI_Old_CD25dual_reverse
Thy1.2+
Freq. of Parent
Geometric Mean : R2-A
99.1 26907
32.9 13035
22.6 14228
10.2 11499
4.43 9677

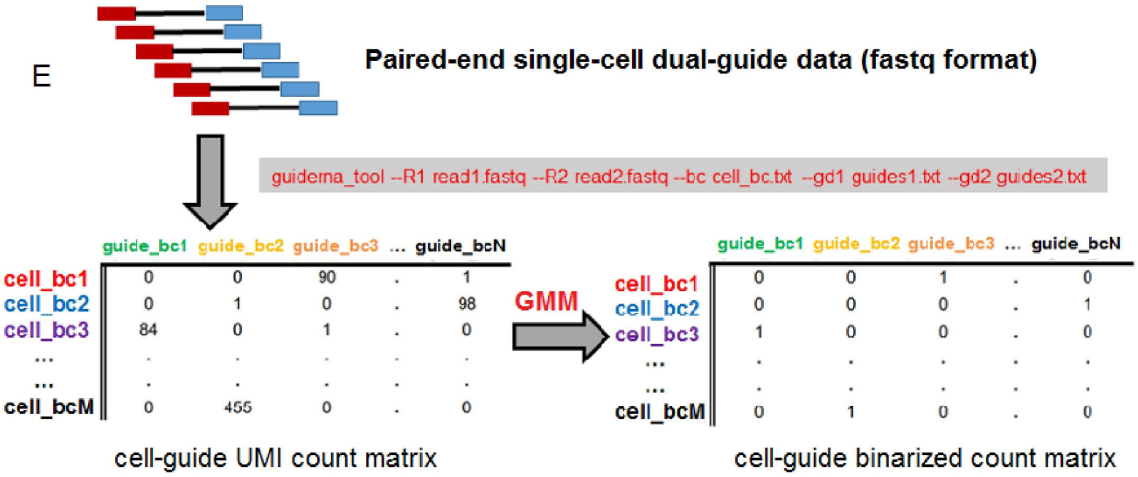
E
Paired-end single-cell dual-guide data (fastq format)
guiderna_tool --R1 read1.fastq --R2 read2.fastq --bc cell_bc.txt --gd1 guides1.txt --gd2 guides2.txt
guide_bc1 guide_bc2 guide_bc3 ... guide_bcN
cell_bc1 0 0 90 . 1
cell_bc2 0 1 0 . 98
cell_bc3 84 0 1 . 0
cell_bcM 0 455 0 . 0
GMM
cell_bc1 0 0 1 . 0
cell_bc2 0 0 0 . 1
cell_bc3 1 0 0 . 0
cell_bcM 0 1 0 . 0
cell-guide UMI count matrix
cell-guide binarized count matrix

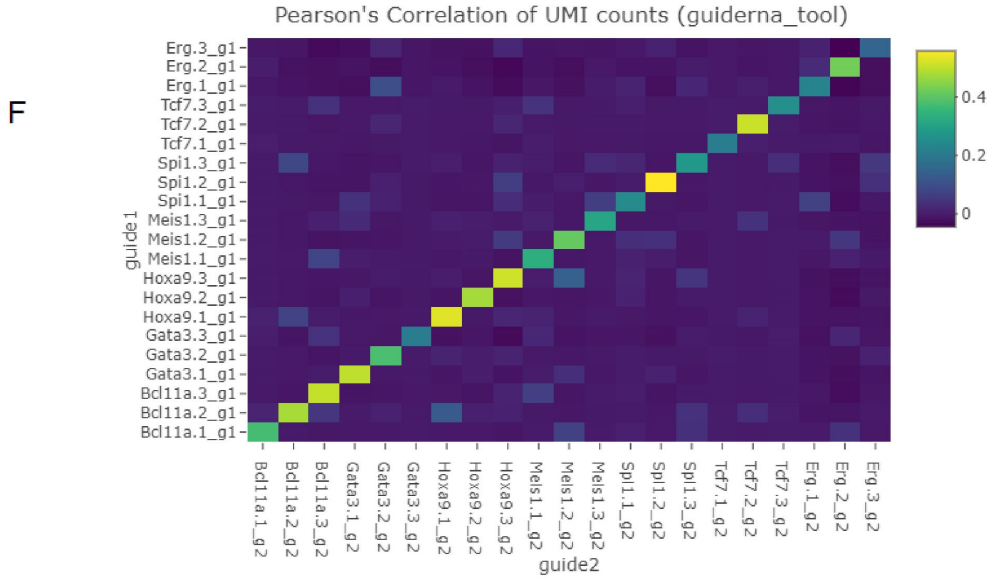
F
Pearson's Correlation of UMI counts (guiderna_tool)
guide1
guide2
Erg.3_g1
Erg.2_g1
Erg.1_g1
Tcf7.3_g1
Tcf7.2_g1
Tcf7.1_g1
Spi1.3_g1
Spi1.2_g1
Spi1.1_g1
Meis1.3_g1
Meis1.2_g1
Meis1.1_g1
Hoxa9.3_g1
Hoxa9.2_g1
Hoxa9.1_g1
Gata3.3_g1
Gata3.2_g1
Gata3.1_g1
Bcl11a.3_g1
Bcl11a.2_g1
Bcl11a.1_g1
Bcl11a.1_g2
Bcl11a.2_g2
Bcl11a.3_g2
Gata3.1_g2
Gata3.2_g2
Gata3.3_g2
Hoxa9.1_g2
Hoxa9.2_g2
Hoxa9.3_g2
Meis1.1_g2
Meis1.2_g2
Meis1.3_g2
Spi1.1_g2
Spi1.2_g2
Spi1.3_g2
Tcf7.1_g2
Tcf7.2_g2
Tcf7.3_g2
Erg.1_g2
Erg.2_g2
Erg.3_g2
0.4
0.2
0

Fig. S12. Technical and analytical details of dual gRNA perturb-seq.

(*A)* The qPCR C_T values of selected vectors from plasmid pool, which sample the evenness of plasmid vector backbones in the cloned dual-gRNA pool. The result showed an evenly synthesized pool of plasmids that was used for viral packaging. Raw ct values can be found in Table S12. (*B)* Multiplicity of infection (MOI) titration with the viral pools containing dual gRNA vectors. All the batches of viral titers were tested separately on primary BM cells, to target precisely MOI of 0.5-1 for the scRNA-seq experiment (viral usage ~ 40-64% of the plateau). Because of the inferior infectivity of pool 3, only pool 1 and pool 2 were used in this study. Raw infection ratios (% CFP+) can be found in Table S12. *(C)-(D)* The validation experiment of dual gRNA effectiveness of acute gene perturbation. *(C)* In response to the low recovery of guide2-cap2 read counts (from pos2 on the illustration), tested directly whether the gRNAs from pos2 were adding effectiveness to the acute perturbation in our system. Here, *Il2ra* (encoding CD25) was targeted by two gRNAs with switching positions. *(D)* Flow cytometry analysis of the dual gRNA validation test. Results shown indicate that the dual gRNA perturbation efficiency towards the same gene was consistently better than a single gRNA. In fact, the same gRNA sequence in pos2 was actually even more effective in perturbation compared to pos1. *(E)* In-house bioinformatic processing pipeline to align the dual gRNA with both Cap1 and Cap2 information (detailed in Methods). *F)* Pearson correlation of UMI counts from guide1 and guide2 assignment.

Supplementary Tables

Tables themselves are submitted as individual datasets.

Table S1. In vivo vs. in vitro T cell development comparison. Bulk RNA-seq Differential Expression analysis comparing corresponding subsets of thymocytes and BM derived pro-T cells, generated under OP9-DLL1 and mATO in vitro differentiation conditions.

Table S2. Genes enriched in each sub-cluster of early pro-T pool-perturbation scRNA-seq. Calculations in this Table are based on Seurat 3 with minimum fraction of expressing cells ≥ 0.25, using Wilcoxon rank sum test with avg_logFC threshold of 0.3 (default pseudocount=1).

Table S3. Differential Expression analysis comparing Control (Cont) and seven TF KOs in early pro-T cell pool-perturbation scRNA-seq. Differentially expressed genes in each comparison of KO to Control were defined with qval < 1E-02, minimum Ln Fold Change ≥ 0.1, minimum fraction of cells expressing ≥ 0.05. Standard for Seurat 3, a pseudocount value of 1 was used for undetected transcripts. These calculations provided the input for Fig. 2B and Fig. 3. DEG lists calculated using alternative criteria giving greater sensitivity to differences in low-level expressed genes are presented separately, in Table S11.

Table S4. SCENIC analysis of pool-perturbation results in Phase 1 cells. (A) SCENIC output of effects from early pro-T cell pool-perturbation scRNA-seq on the complete set of regulons scorable in this dataset. Mean and median AUC values are shown, and differences between means and control means as fraction of the control means. (B) Regulon target gene lists in this dataset. Note that SCENIC analysis is based on calculations from the primary data that are completely independent of the Differential Expression analyses. (C) D values (difference) between regulon activities in different knockouts relative to control. (D) Kolmogorov-Smirnov p values for differences between regulon activities in different knockouts relative to controls.

Table S5. Characterization of gene expression subclusters in WT and Bcl11b KO samples. (A) Marker genes for all subclusters in Integrated WT and Bcl11b KO scRNA-seq analysis; adjusted pval <1E-02. (B) Proportion represented by each subcluster in each of the D10 and D13 WT and Bcl11b KO samples.

Table S6. Differential gene expression analysis between D10 and D13 timepoints in WT and Bcl11b KO. Data here were pooled from single-cell data to give “pseudo-bulk” comparisons. DEG criteria as in Table S3.

Table S7. Differentially expressed genes between specific Clusters in WT and Bcl11b KO scRNA-seq analysis. (A) Differentially expressed genes between Cluster 0 and Cluster 2 in integrated WT and Bcl11b KO scRNA-seq analysis. (B) Genotype-based differential expression analysis (WT vs. Bcl11b KO) within shared Cluster 5. DEG criteria as in Table S3.

Table S8. SCENIC analysis of Bcl11b KO effects. (A) SCENIC analysis of regulon effects of Bcl11b KO as compared to WT at D10 and D13 of culture. Mean and median AUC values for each regulon are given. Below, (1) differences calculated between each regulon mean in KO as compared to D10 WT controls, (2) differences calculated between each regulon mean in KO as compared to same-day WT controls, and (3) Fold Differences calculated between each regulon AUC value at each timepoint and the AUC value of the WT at D10. (B) Regulon target gene lists from this dataset. (C) D values (difference) between regulon activities in different knockouts relative to the indicated comparators. (D) Kolmogorov-Smirnov p values for differences between regulon activities in different knockouts relative to the indicated comparators.

Table S9. Gene lists and statistics for gene network predictions based on the regulon-DEG intersection genes. (A) Curated PU.1 responsive DEGs and their overlap with genes in the Spi1 regulon. (B) Definition of Bcl11b-restrained program: curated Bcl11b KO DEGs and overlap of these DEGs with members of regulons enriched in Bcl11b KO samples (Table S8): gene lists and statistical significance of DEG intersection. TF coding genes are in bold, chromatin modifier genes are in bold italic. (C) Input-target matrix for Bcl11b-repressed regulon-DEG intersect genes: data for Fig. 8A. (D) Definition of the Phase 1 T-

lineage progression program. Overlap of curated PU.1-repressed DEGs with members of regulons enriched in Spi1 KO samples (Table S4): gene lists, statistics of enrichment (cf. Fig. 8B); and enrichment of same regulons in other pool-perturbation KO samples. (E) Input-target matrix for PU.1-repressed regulon-DEG intersect genes: data for Fig. 8C. (F) Identities of individual Phase 1 “progression” regulon member genes that intersect with PU.1-activated rather than PU.1-repressed DEGs. (G) Relationship of Phase 1 “progression” regulons to later programs controlled by Bcl11b: genes in the same regulons overlapping with Bcl11b-repressed or Bcl11b-activated DEGs from ref. (*37*).

Table S10. Designed gRNA list (A) and pool oligo list (B) used for generating pool-perturbation dual gRNA vectors.

Table S11. Differential Expression analysis in early pro-T cell pool-perturbation scRNA-seq using an alternative method to increase sensitivity to low levels of expression. To increase accuracy of fold change determinations, calculations in this Table are based on use of a lower pseudocount floor value for undetected transcripts (pseudocount=0.01), with qval < 1E-02 and fraction of cells expressing $\geq$ 0.05. To offset the contribution of low-expression noise, the minimum ln Fold Change was increased to $\geq$ 0.2.

Table S12. Table of raw data. Shown are raw demultiplexed cell number data from pool-perturbation analysis, cells with each guide RNA pair reported separately (Fig. 2F); cluster proportions in CRISPR pool-perturbation analysis, separated by targeted gene (Fig. 2G); qPCR verification of guide RNA plasmid representation in original library (Fig. S12A); virus-packaged library measured titers (Fig. S12B); and cluster proportions in CRISPR pool-perturbation analysis, cells with each guide RNA pair tracked individually (Fig. S4C).